Study on Single-Photon Detection by Silicon-On-Insulator Metal-Oxide-Semiconductor Field-Effect

静岡大学　博士論文

シリコン・オン・インシュレーター金属酸化膜半導体電界効果

トランジスタによる単一光子検出の研究

プトラント　デディ

静 岡 大 学

大学院自然科学系教育部

ナノビジョン工学専攻

2014 年 12 月

DOCTOR THESIS

Study on Single-Photon Detection by Silicon-On-Insulator Metal-Oxide-Semiconductor Field-Effect Transistor

Dedy Septono Catur Putranto

Graduate School of Science and Technology

Shizuoka University

Japan

December 2014

DOCTOR THESIS

Study on Single-Photon Detection by Silicon-On-Insulator Metal-Oxide-Semiconductor Field-Effect Transistor

シリコン・オン・インシュレーター金属酸化膜半導体電界効果トランジスタによる単一光子検出の研究

Dedy Septono Catur Putranto

Student No: 55145029

Graduate School of Science and Technology

Shizuoka University

Japan

2014

Study on Single-Photon Detection by Silicon-On-Insulator Metal-Oxide-Semiconductor Field-Effect Transistor

シリコン・オン・インシュレーター金属酸化膜半導体電界効果トランジスタによる単一光子検出の研究

By

Dedy Septono Catur Putranto

Diploma of Cryptography

National Crypto Academy (AKSARA), Bogor, Indonesia (2003)

Bachelor of Engineering

Electrical Engineering Department, Faculty of Engineering

Universitas Pancasila, Jakarta, Indonesia (2005)

Master of Engineering

Electrical Engineering Department, Faculty of Engineering

Universitas Indonesia, Depok, Indonesia (2011)

Thesis submitted to Graduate School of Science and Technology, in partial fulfillment of the requirements for the degree of Doctor of Engineering at Shizuoka University, Japan (2014)

Advisory Committee:

Professor Hiroshi Inokawa, Supervisor

Professor Michiharu Tabe, Chairman

Professor Jun Kondoh

Professor Djoko Hartanto

Professor Hiroya Ikeda

Abstract

A single hole sensitivity operation has the unique property of directly detection photo-generated carriers one by one, which makes silicon-on-insulator (SOI) metal-oxide-semiconductor field-effect transistor (MOSFET) single-photon detector promising for novel function electronics operating at room temperature. Some prospective type single photon detector based on a scaled-down (gate length L= 65 nm and channel width W= 105 nm) SOI MOSFET, which features improved quantum efficiency (QE), low dark counts and higher operation speed. However, in these devices, a special double-gate structure with a short lower gate (LG) and a long upper gate (UG) covering the entire p-doped SOI area was used to create potential well below the LG to trap photo-generated holes. This complex structure resulted in still low QE, and might be an obstacle to general use. A simple structure of SOI MOSFET that can be found in ordinary integrated circuits is evaluated as a single-photon detector. A potential well created by $n^+p^-n^+$ junctions is used to trap photo-generated holes, and the presence of the holes is detected as increased electron current in the top or bottom channel. In this background, it is attractive to observed novel function of SOI MOSFET with different structure.

In this thesis, analysis of hole lifetime SOI MOSFET single-photon detector 1), effect of substrate voltage SOI MOFSET single photon detector on noise and hole lifetime 2) and novel function of SOI Fin-type field effect transistor as single photon detector 3) is demonstrated. Low-frequency noise and hole lifetime in SOI MOSFET are analyzed, considering their use in photon detection based on single-hole counting. The noise becomes minimum at around the transition point between front- and back-channel operations when the substrate voltage is varied, and increases largely on both negative and positive sides of the substrate voltage showing peculiar Lorentzian (generation-recombination) noise spectra. Hole lifetime is evaluated by the analysis of drain current histogram at different substrate voltages. It is found that the peaks in the histogram corresponding to the larger number of stored holes become higher as the substrate bias becomes larger. This can be attributed to the prolonged lifetime caused by the higher electric field inside the body of SOI MOSFET. It can be concluded that, once the inversion channel is induced for detection of the photo-generated holes, the small absolute substrate bias is favorable for short lifetime and low noise, leading to high-speed operation.

Dark and maximum count rates are quantitatively correlated to device performances. From Simulation result the state-of-the-art charge sensor can realize maximum count rate of 7.6 Ms^{-1}, dark count rate of

0.01 s^{-1}, and the dynamic range of 178 dB with charge sensitivity of 10^{-5} e/$\sqrt{}$Hz.

In the SOI fin-type field effect transistor (FinFET) with multigate structure was investigated as a photon detector. We could successfully confirm the photodetection capability, in that the drain current histogram evolved toward the high-current side as the light intensity increased, reflecting the accumulation of photogenerated holes. Although the QE improved to 9.0% at λ= 400 nm, we could not attain better charge sensitivity or dynamic range as a photon detector. Further investigation in device structure and dimensions for higher charge sensitivity is anticipated.

The ability SOI MOSFET to detect single photon by single hole sensitivity at room temperature can be useful in the integrated circuit for future application. For practical applications, however, higher quantum efficiency should be addressed which will require further study beyond the purpose of this present thesis.

Acknowledgement

Al-hamdulillahirabbil 'alamin, after spending three years working with wonderful people, now is the time for me express my gratitude to all of people who made this thesis accomplished.

First of all, I would like to express with deepest respect and my profound gratitude to my supervisor, Prof. Hiroshi Inokawa, who gave me an opportunity to challenge a research project in the present state of the art the nano electronics technology under his supervision. I am very grateful to him, for his support and encouragement. He always impressed me with his vast knowledge, wide experience, deep thinking, understandable explanation and low profile personality. I have learned a lot from him about how to combine to smartness and kindness, great dream and patience, as well as professionalism and humbleness at the same time, making me feel very fortunate to work under his guidance.

I would like to express with deepest respect and my profound gratitude to my supervisor at University of Indonesia, Prof. Dr. Ir. Djoko Hartanto, M.Sc. and Dr. Ir. Purnomo Sidi Priambodo, M.Sc. for they support before and during my Ph.D. work.

I also would like to thank the committee members of my Ph.D., Prof. Michiharu Tabe, Prof. Jun Kondoh, Prof. Hiroya Ikeda for their invaluable comments and suggestions in improving this thesis.

I would like to express grateful to Dr. M. Masahara and researchers in National Institute of Advanced Industrial Science and Technology (AIST) for providing devices for evaluation.

I would like to thank all my colleagues (Dr. Hiroaki Satoh, Dr. Atsushi Ono and Dr. Wei Du) and my friend (Dr. Tiwari Ajay, Mr. Shuu Takeuchi, etc.) in the Nanosystem Integration Laboratory. Thank you very much for being my great tutors and friends. It is difficult for me to imagine spending three years without their tutoring, friendship and support.

Finally, I would like to express my great gratitude to my beloved parent Mr. Budi Hermani and Mrs. Siti Koyimah for their continuous love and blessing, for their wisdom and their pray during the day and the night. My great gratitude extends to my parent in law Mr. Sudjadi and Mrs. Lilik Purwati and all my brothers and sisters for them support and advice.

My beloved wife Rini Wisnu Wardhani, S.T., M.T. for her patient and love coming into my life, sharing the warm love and giving me a lovely daughter, Rafifah Nur Aida Putranti. May Allah Subhana wata'ala reward them with best rewards. Thanks to Rafifah Nur Aida Putranti, her pray and patient always giving me a positive energy. To all of them this thesis is dedicated.

Hamamatsu, December 2014

Dedy Septono Catur Putranto

Table of Contents

Table of Figures

Chapter 1

INTRODUCTION

1.1   Research Background

The detection of single quanta of electromagnetic radiation has been traditionally motivated by applications such as materials characterization, medical imaging and diagnosis, chemical analysis and far-infrared spectroscopic research. Over the last two decades, through the merger of concepts in classical information theory and quantum physics has emerged the new field of "quantum information science", which in turn has brought forth new technologies such as quantum computing [1] and quantum cryptography [2]. Quantum information technologies promise unparalleled information processing and secure telecommunications capabilities. With the emergence of these new technologies, the need has arisen to perform more than just the detection of the individual quanta of electromagnetic energy. For example, quantum cryptography relies for security on the quantum uncertainty principle by encoding information onto the intrinsic quantum states of single photons. Hence, it is required for single-photon detectors to

perform more than just detect the presence or absence of a single photon; they need to have the additional capability of providing a read-out mechanism for the quantum states of single photons over a quantum tele-communication channel. The long distance transmission of quantum information requires unconventional regeneration techniques, which involve the sharing of polarization entangled pairs of photons across the telecommunication channel. At every repeater node, a detector must be made available that detects the successful arrival of one photon of an entangled pair in a non-invasive way preserving the polarization information.

Conventionally, single photons are detected by the multiplication of a photogenerated carrier through an avalanche gain process, either in a vacuum photomultiplier tube, or, in the case of the semiconductor avalanche photodiode, a reverse biased junction.

On the other hand the performance of a single-photon detector is characterized by several important parameters such as quantum efficiency (QE), dark count rate, maximum count rate and noise equivalent power (NEP). Performances of conventional single-photon detector are limited due to carrier multiplication by high electric field, the long recovery time and after pulses, etc.

Due to the progress in integrated circuit technology, scaled down solid-state devices are drawing attention as a single-photon detector based

on single charge counting, we can expect better performances if we directly counts photo-generated carriers one by one without multiplication because operation speed is not limited by recovery time and after pulse cause by carrier multiplication.

Several examples of conventional of single-photon detector and single-photon detector based on single-charge counting such as photo multiplier tubes, avalanche photodiode, single-photon avalanche diode, photodetector based on single-charge counting have been proposed and will be shortly summarized in the following.

1.2   Conventional Single-Photon Detectors

Historically, single-photon detection devices started after the invention of photomultiplier tubes (PMTs) in 1930s [3]. The first solid-state single-photon detection was based on avalanche photodiodes (APDs) and was invented in early 1960s [4]. Single-photon avalanche diodes for visible-photon range were realized in 1984 [5]. Nowadays, there are several types of single-photon detection devices. Here, some of the most common devices will be summarized.

1.2.1 Photomultiplier Tubes (PMTs)

Photomultiplier Tubes (PMTs) are vacuum tubes which utilize the photoelectric effect and internal gain mechanisms to produce a current in response to low light levels. Incident photons on the photocathode produce electrons as shown in Fig. 1-1. [6] These electrons are accelerated and focused on the first dynode and multiplied via secondary electron emission. These secondary electrons are accelerated towards the second dynode and subsequently multiplied. After multiple stage dynode amplification, the electrons are collected by the final anode and the current is read out.

The problems in operation principle of PMTs are related to the carrier multiplication by high electric field such as electron transit time, high-voltage operation, incompatibility with magnetic field and amplitude fluctuation, and PMTs also cannot resolve photons when multiple photons enter at the same time because the linearity of output signal cannot representative number input of multiple photon, it related to small sensitivity of detector.
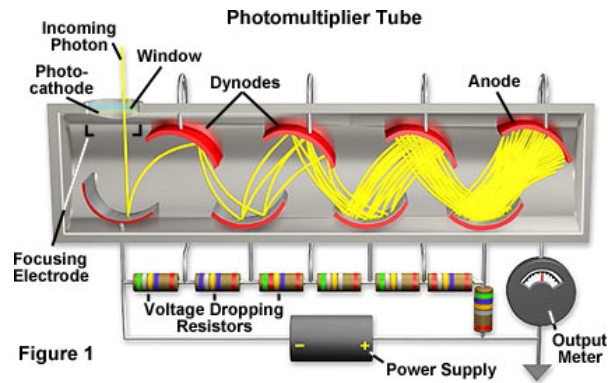
Figure 1-1 Schematic view of a photomultiplier tube.

1.2.2 Avalanche Photodiodes (APDs)

Avalanche Photodiodes (APDs) are semiconductor based photodetectors that utilize an internal gain mechanism through applying a reverse bias voltage. Because of this internal gain mechanism, APDs are useful in detecting low light levels and used in a variety of applications. APD structures are typically p-n junctions or p-i-n junctions as shown in Figure 1-2. [7]

When a photon enters the photodiode, an electron-hole pair is generated if the energy of the photon is greater than the band gap of the material. When the electron hole pair is generated in the depletion region of the p-n junction, they are subsequently separated from each other by the electric field generated by the reverse bias voltage, with electrons drifting towards the n^+ side and holes drifting towards the p^+ side. Because of the high electric field, the electrons and holes are accelerated

and can collide with the crystal lattice with enough energy to create a secondary electron-hole pair. This phenomenon is termed impact ionization. These secondary electron-hole pairs can generate subsequent electron-hole pairs in a so-called avalanche process. Impact ionization begins at electric field strengths of $>10^5$ V/cm. [7]
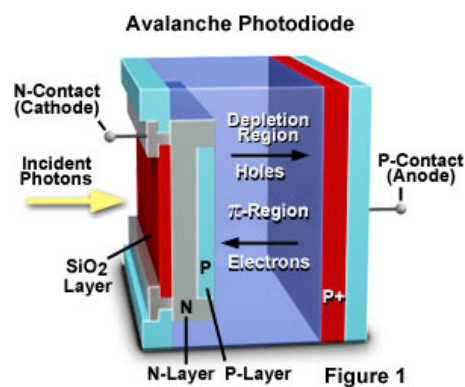
Figure 1-2 Cross-section of an avalanche photodiode.

1.2.3 Single-Photon Avalanche Photodiode (SPAD)

A single-photon avalanche diode (SPAD) is a variant of APD with Geiger-mode operation, in which a photo-generated carrier can trigger an avalanche current due to the impact ionization mechanism. This device structure based on solid-state p-n diode structure is used, as shown in Fig. 1-3. [8] The fundamental difference between SPAD and APD is that SPADs are specifically designed to operate with a reverse-bias voltage

well above the breakdown voltage, whereas APDs operate below the breakdown voltage.

When biased above the breakdown voltage, by definition, electron-hole pairs are generated on average faster than they can be extracted. Hence, when a photon impinges on the photodiode and is absorbed in the depletion region, an electron-hole pair will be generated, and a self-sustaining runaway avalanche process will occur. Immediate quenching of the runaway charge is necessary to prevent damage to the photodiode and this forms a short current pulse indicating the detection of a single photon. This avalanche pulse acts as a binary signal, whether or not a photon was detected, unlike the analog signal obtained from electron multiplication in APDs. Quenching can be achieved through a simple passive quenching resistor or through more complex active quenching circuits. Important SPAD figures-of-merit include detection probability, spectral response, dark count rate, timing precision (jitter), sampling speed, active area and fill factor.

SPADs have a difficulty in resolving number of photon related to binary output signal cannot representative number of multiple input of photon.
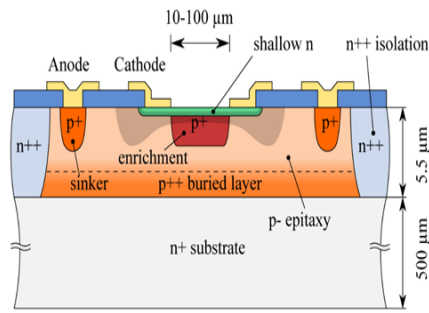
Figure 1-3 Schematic view of a single photon avalanche diode.

1.3 Single-Photon Detector based on Single-Charge Counting

1.3.1 Photodetector based on metallic SET

In 1992 A. N Cleland et al. demonstrated photo detection based on single-electron transistor (SET) electrometer with an intrinsic noise of far less than one electron per unit bandwidth at 20 mK using device structure as shown in Figure 1-4 [9], where SET consists of ultra small planar tunnel junctions connected in series. The entire device was fabricated on an oxidized p-type Si chip with a room-temperature resistivity of 6 Ω cm, corresponding to a boron doping density of $2 \times 10^{15}/cm^3$. The oxide layer was 450 nm thick, and no electrical contacts were made to the Si substrate.

By assuming an ideal detector with a collection efficiency of $\eta = 1$, the dark current corresponds to a minimum light flux of $\Gamma = 0.06$ photons/s. For infrared light with $\lambda = 30$ μm, the calculated noise-equivalent power would be NEP = $(hc/\lambda)(2\Gamma)^{1/2} = 2\times10^{-21}$ W/$\sqrt{\text{Hz}}$, and the corresponding detectivity for this detector with area A= 300 μm^2 would be D* = $\sqrt{A}$/NEP = 8×10^{17} cm*$\sqrt{\text{Hz}}$ /W.
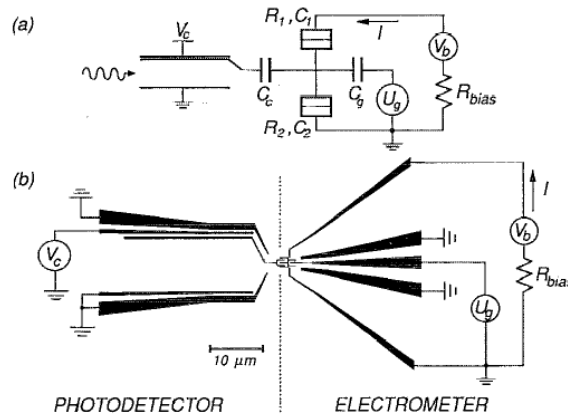
Figure 1-4 (a) Circuit diagram for the experiment, (b) Geometrical layout of the metallic parts, deposited on the photon-absorbing Si substrate. [9]

1.3.2 Photodetector based on GaAs 2DEG SET

Single-photon counting at microwave frequencies around 500 GHz is demonstrated by O. Astafiev et al. in 2002 [10], this device is using a single-electron transistor (SET) formed by two capacitively coupled GaAs/Al$_x$Ga$_{1-x}$As single-heterostructure crystal with a two-dimensional

electron gas (2DEG) of a sheet density of n_s = 0.9x10^{15} m^{-2} and a mobility

of μ = 190 m^2/V s (T = 4.2 K). The sample is an SET consisting of double

QDs as represented in Fig. 1-5(a). The dark switch rate (W_{DS}) is 0.01 s^{-1}

and quantum efficiency (QE) is 0.1%, and the noise equivalent power

(NEP) is the order of 10^{-21} W/Hz$^{1/2}$, which is consistent with the estimated

intensity of incident radiation.
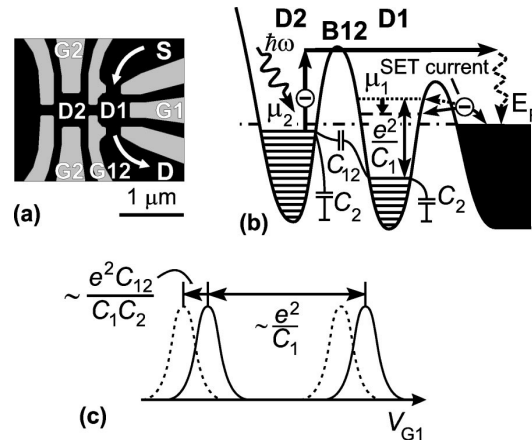
Figure 1-5 (a) Top view of a double-QD photon detector, (b) Schematic representation of photo excitation mechanism, (c) Conductance oscillation and a peak shift caused by single photoexcitation event. [10]

1.3.3 Photodetector based on Si 2D MTJ FET

A single-photon detection using a Si-based two-dimensional (2D) multiple-tunnel-junction (MTJ) field-effect transistor (FET) is reported in 2006 by R. Nuryadi et al. [11] Figure 1-6 show schematic view of a 2D Si multidot channel FET, single photon is detected as a random telegraph

signal in the single-hole tunneling current regime at operation temperature 15 K, where the frequency of RTS events depends on the light wavelength and intensity.

A Monte Carlo simulation using an equivalent 2D circuit consisting of 7x8 dots shows that the on state of RTS appears when the photon is absorbed in the dot and its charging effect influences the current, while the off state of RTS appears when the charged dot is neutralized. It is also found that, for sufficiently large screening lengths, RTS is triggered not only by the charging of the dots adjacent to the current percolation path, but also by the charging of the dots away from the path. These results provide a possibility of developing the single-photon detector using 2D dots system.

(a)   (b)
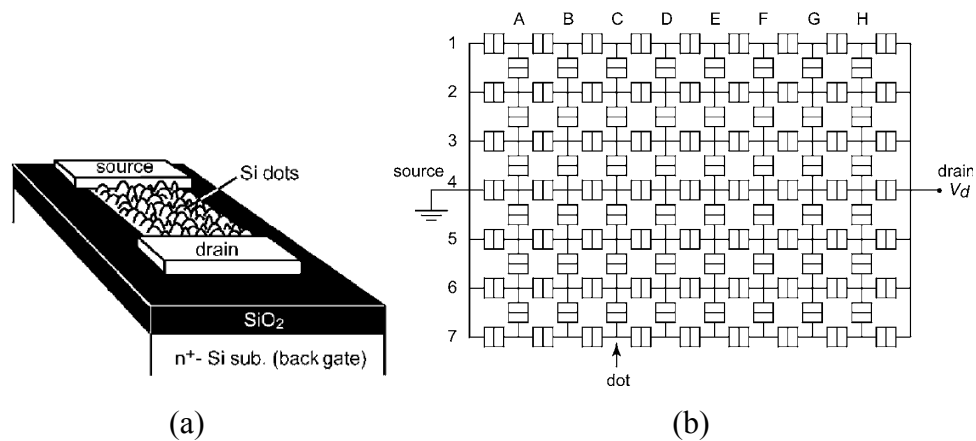
Figure 1-6 (a) Schematic view of a 2D Si multidot channel FET. (b) Equivalent circuit of the 2D tunnel junction array consisting of 7x8 dots used in the simulation. [11]

1.3.4 Photodetector based on GaAs 2DEG FET gated by layer of quantum dots

The operation of quantum-dot-based photon detector that relies on the coulomb interaction resulting from trapping of photo excited carrier by quantum dot is reported by A. J. Shields in 2000. This coulomb interaction is detected as a change of the source-drain current in a transistor at 4 K. Schematic device structure and SEM image of gate of quantum dot field-effect transistor-based single-photon detector is shown in Fig. 1-7 [12]. It consists of a GaAs/Al0.33Ga0.67As modulation-doped FET containing a layer of InAs quantum dots separated from the 2DEG in the GaAs channel by a thin Al0.33Ga0.67As barrier.

Illumination creates electron–hole pairs within the structure. Holes photoexcited in the quantum well are swept by the internal electric fields towards the negatively charged dots. After tunneling into the quantum dot they recombine with excess electrons trapped there. Meanwhile, the photoexcited electron remains in the 2DEG layer. Thus, illumination reduces the number of electrons trapped within the dots, with a corresponding increase in the 2DEG density.
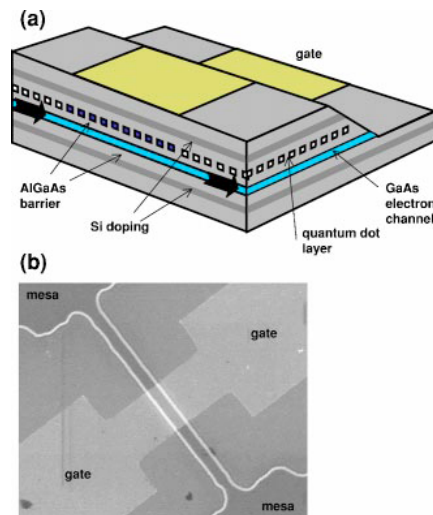
Figure 1-7 (a) Schematic of the quantum-dot FET structure, (b) SEM image of gate region. [12]

1.3.5 *Photodetector based on Si GC FET*

In 2007 Nishiguchi et al., demonstrated IR sensing using a Gain Cell (GC) at room temperature as shown in Fig. 1-8.[13] The GC has functions of electrically controlled short-wavelength pass filter and sensitivity, which will be useful for material analysis applications in which a particular IR wavelength must be cut or picked up. The IR signal excites conduction-band electrons in an undoped channel of a MOSFET and some of them are injected through an energy barrier into a storage node (SN) electrically formed by the MOSFET. Small signals, originating from electrons, stored in the SN are detected by an electrometer with a single-electron resolution.
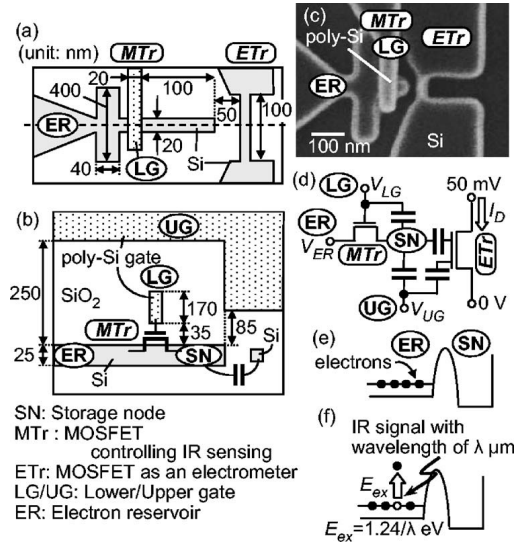
Figure 1-8 (a) Schematic top view, (b) Cross-sectional view, (c) SEM image, (d) Equivalent circuit, (e) Energy band diagram without IR signal, and (f) Energy band diagram when IR signals are irradiated. [13]

1.3.6 Photodetector based on Si nanowire FET

Detection of single electrons and single holes is demonstrated at room temperature in Si nanowire transistors using an electron-hole (e–h) system as shown in Figure 1-9. [14] Photogenerated carriers are stored in a quantum dot electrically formed in a Si wire by a front gate. The stored charges affect the current of the other type of carriers that flow along the bottom of the Si wire.

From the Si thickness 30 nm and detector area 64 μm^2, the efficiency of light absorption was estimated to be 1.4% at $\lambda = 650$ nm. The efficiency of collecting holes into the Si wire was then calculated to

be 0.9% from the present data. In spite of the resultant poor quantum efficiency of 0.013%, the background τ_g^{-1} of 0.012 s^{-1} leads to noise-equivalent power as low as 7x10^{-15} W at 1 Hz and 2x10^{-17} W at 10^{-3} Hz, which are comparable to those of commercially available photodetectors.
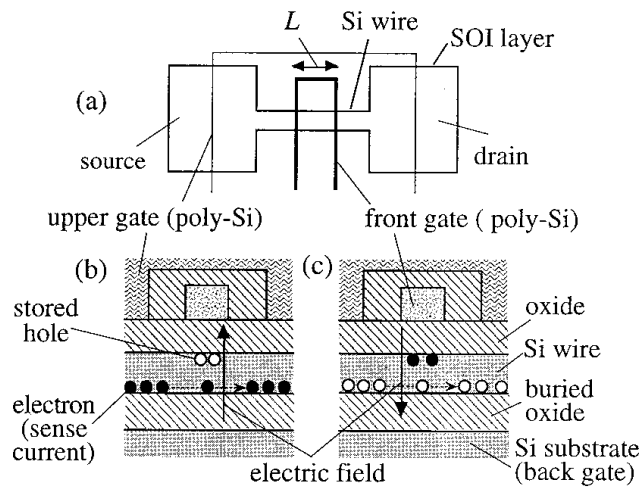
Figure 1-9 (a) Schematic top view of the Si-wire MOSFET, (b) Schematic cross section of the device along the Si wire for the *n*-channel MOSFET, (c) Schematic cross section for the *p*-channel MOSFET. [14]

1.4 Motivation of Present Work

As described before the issues in conventional PMT and APD, such as dark counts, operation speed limited by the recovery time and after pulses, high operation voltage, etc. can be solved by photodetector based on single-charge counting because of the direct detection of photo-

generated carriers one by one without any multiplication. However, the reported devices still have issues in QE, operation speed, temperature, etc. Such issues are addressed in this thesis in several aspects such as noise, lifetime of stored charge, charge sensitivity related to device structure, expected quantitative performance, etc. The benchmark comparison single-photon detectors are compared in Table 1.1. Our study is focusing on single-charge-counting-based single-photon detectors at room temperature with low dark count <0.01/s and maximum count rate >300/s.

Tabel 1.1 Benchmark comparison of single-photon detectors

	PMT		APD		SPAD		SSPD		Single charge counting
	Visible-near infrared [15]	Infrared [16]	Si [17]	InGaAS [18]	Si [19]	InGaAS [20]	SSPD [21, 22]	TES [23, 24]	Si nanowire FET [14]
Dark count rate	100 Hz	200 kHz	<25 Hz	<10^4	25 Hz	91 Hz	<0.01	<0.001	<0.01
Max. count rate	10 MHz	10MHz	10 MHz	1 MHz	10 MHz	10 MHz	250 MHz	20 kHz	10 Hz
Quantum efficiency, η	40% @500nm	2% @1550nm	70% @630nm	25% @1550nm	49% @550nm	10% @1550nm	10% @1550nm	92% @1550nm	0.013% @650nm
Wavelength	300-720nm	300-1700nm	400-1100nm	900-1700nm	375-1000nm	300-1700 nm	400-5600nm	100-5000nm	650nm
Light receiving area	5 mm	3x8 mm	170 µm	300x250x 150 mm	20 µm	25 µm	10x10 µm	25x25 µm	64 µm^2
Timing resolution	300 ps	300 ps	300 ps	300 ps	35 ps	370 ps	18 ps	300 ns	-
Operation magnetic field	No	No	Yes	Yes	Yes	No	No	No	Yes
Photon-number resolution	Very limited	Very limited	Very limited	No	No	No	Study in progress	Yes	Yes
Operation temperature (K)	300	200	300	200	200	200	2-4.2	0.1	300

Here we research on single-photon detection based on SOI MOSFET with single-hole sensitivity [25, 26], focusing on several main points:

1.   Optimization of the operation conditions related to the speed performance. For this purpose, behavior of the drain current noise and the hole lifetime is analyzed in terms of substrate bias dependence.

2.   Clarification of the required SOI MOSFET characteristics in order to attain the target dark count and maximum count rates. Charge sensitivity in the unit of $e/\sqrt{Hz}$ is introduced to quantitatively show the requirement.

3.   Evaluation of the SOI FinFET for improved charge sensitivity, leading to higher performance in terms of dark count and maximum count rate.

This study may provide the ground for developing the SOI MOSFET single-photon detector that can really outperform and replace the existing detectors.

1.5   Synopsis of Book Chapters

This thesis consists of five chapters correspond to research approach as shown in Figure 1-10, summarized in following paragraphs.

Research Approach
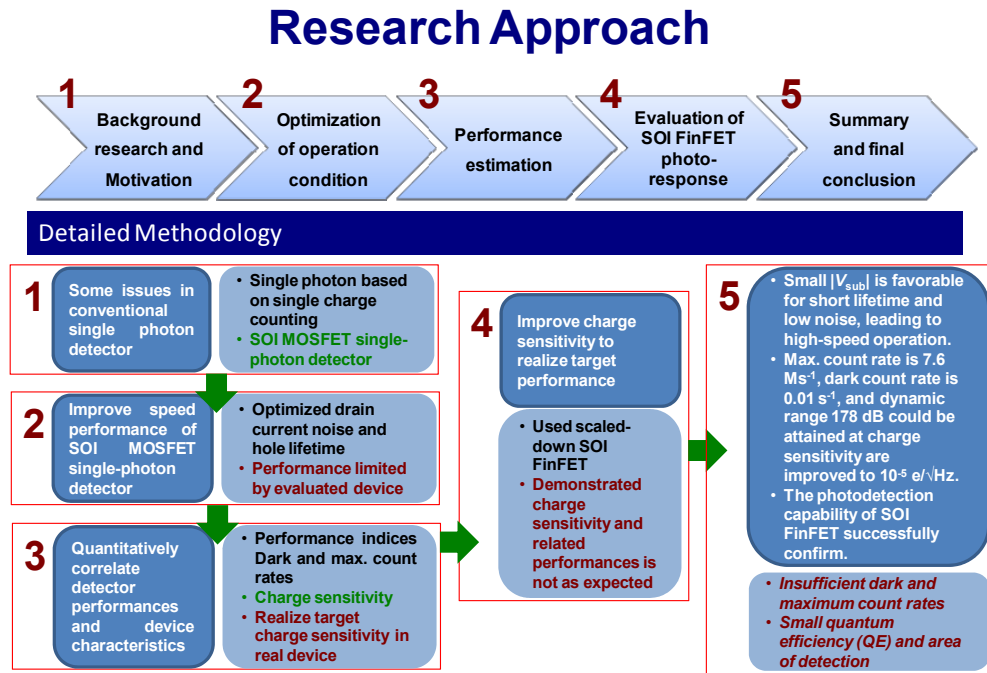
Figure 1-10 Structure of dissertation corresponding to methodologies of research.

In chapter 1, the background of the research related to single-photon detector is described. Some conventional single-photon detectors and other single-photon detectors based on single-charge counting are summarized. Motivation of the present research is outlined and synopsis each chapter is also given.

In chapter 2, optimization of the operation conditions related to the speed performance is described. Specifically, the drain current noise and hole lifetime, which determine the maximum count rate, are analyzed. Evolutions of the noise spectra under dark conditions, and the hole

lifetime extracted from the drain current histogram under different illumination levels are evaluated with respect to the substrate bias.

In chapter 3, Performance of the SOI MOSFET photon detector is estimated based on the simulated output waveforms based on the Poisson processes in photon incidence and hole recombination, and the signal processing algorithm for detecting the events. From the series of simulations for various hole generation rates, noise levels and sampling frequency for signal processing, required SOI MOSFET characteristics to attain the target dark count and maximum count rates are clarified. The requirement is described as charge sensitivity in the unit of $e/\sqrt{Hz}$.

In chapter 4, In order to improve the charge sensitivity, SOI fin-type field-effect transistor, which is expected to have higher immunity to the short-channel effect, is introduced and evaluated as a photon detector. Experimental results and discussion related to drain current waveform under dark and illuminated conditions are described. Analysis of the drain current histogram reveals the charge sensitivity, hole generation rate and hole lifetime, indicating the potentials of the FinFET as a photon detector.

Chapter 5 contains the summary and conclusions of this research and provides suggestion on the direction for future development in this area.

References

[1]   Isaac L. Chuang and Neil Gershenfeld, "Quantum Computing with Molecules," *Scientific American*, pp. 66-71, 1998.

[2]   Simon Singh, "The Code Book: The Science of Secrecy from Ancient Egypt to Quantum Cryptography", *Delacorte Press*, New York, 2002.

[3]   Z. Bay, "Electron Multiplier as an Electron Counting Device," *Nature*, 141, pp. 1011-1011, 1938.

[4]   R. J. McIntyre, "Theory of Microplasma Instability in Silicon," *J. Appl. Phys.*, 32, pp. 983-995, 1961.

[5]   D. E. Groom, "Silicon photodiode detection of bismuth germinate scintillation light," *Nucl. Instrum. Methods Phys. Res.*, 219, pp. 141-148, 1984.

[6]   Hamamatsu Photonics K.K. Editorical Committee, "*Hamamatsu Photomultiplier Tubes - Basics and Applications*," Hamamatsu Photonics K.K. Electron Tube Division, Third Edition, pp. 14-17, 2007.

[7]   Hamamatsu Photonics K.K, "*Characteristics and use of Si APD (Avalanche Photodiode)*." SD-28. KAPD9001E03, 2004, URL: http://www.hamamatsu.com/resources/pdf/ssd/si_apd_techinfo_e.pdf.

[8]   M. D. Eisaman, J. Fan, A. Migdall, and S.V. Polyakov, "Invited review article: Single photon sources and detectors", *Rev. Sci. Instrum.*, 82, p. 071101, 2011.

[9]   A. N. Cleland, D. Esteve, C. Urbina and M. H. Devoret, "Very low noise photodetector based on the single electron transistor," *Appl. Phys. Lett.* 61(23), pp. 2820-2822, 1992.

[10]   O. Astafiev, S. Komiyama, T. Kutsuwa, V. Antonov, Y. Kawaguchi and K. Hirakawa, "Single-photon detector in the microwave range," *Appl. Phys. Lett.*, 80(22), pp. 4250-4252, 2002.

[11]   R. Nuryadi, Y. Ishikawa and M. Tabe, "Single-photon-induced random-telegraph-signal in a two-dimensional multiple-tunnel-junction array," *Phys. Rev. B,* 73(4), pp. 045310-1-045310-7, 2006.

[12]   C. Santori, M. Pelton, G. Solomon, Y. Dale, and Y. Yamamoto, "Triggered Single Photons from a Quantum Dot," *Phys. Rev. Lett.*, 86, pp. 1502-1505, 2001.

[13]   K. Nishiguchi, Y. Ono, A. Fujiwara, H. Yamaguchi, H. Inokawa, and Y. Takahashi, "Infrared detection with silicon nano-field-effect transistors, " *Appl. Phys. Lett.* 90(22), pp. 223108-1-223108-3, 2007.

[14]   A. Fujiwara, K. Yamazaki, and Y. Takahashi, "Detection of single charges and their generation-recombination dynamics in Si

nanowires at room temperature," *Appl. Phys. Lett.*, 80(24), pp. 4567-4569, 2002.

[15] http://jp.hamamatsu.com/resources/products/etd/pdf/m-h7422e.pdf.

[16] http://jp.hamamatsu.com/resources/products/etd/pdf/NIRPMT_AP PLI_ TPMO1040E02.pdf.

[17] SPCM-AQR-16-FC-Si APD single photon counting module with <25 dark counts/second (2007). [Online]. Available: http://www.perkinelmer.com/CMSResources/Images/44-12462DT S_SPCM%20AQRH. pdf.

[18] id201 (2007). [Online]. Available: http://www.idquantique.com

[19] Micro Photon Devices. PDM series datasheet. http://www.micro-photon-devices.com/Docs/Datasheet/PDM.pdf.

[20] C. Gobby, Z. L. Yuan, and A. J. Shields, "Quantum key distribution over 122 km of standard telecom fiber,"*Appl. Phys. Lett.* 84, pp. 3762–3764, 2004.

[21] A. Korneev, V. Matveinko, O. Minaeva, I. Milostnaya, I. Rubtsova, G. Chulkova, K. Smirnov, B. Voronov, G. Gol'tsman, W. Slysz, A. Pearlman, A. Verevkin, and R. Sobolewski, "Quantum efficiency and noise equivalent power of nanostructured, NbN, single-photon detectors in wavelength range from visible to infrared," *IEEE Trans. Appl. Supercond.*, 15, 2, pp. 571-574, 2005.

[22] A. Korneev, P. Kouminov, V. Matvienko, G. Chulkova, K. Smirnov, B. Voronov, G. N. Gol'tsman, M. Currie, W. Lo, K. Wilsher, J. Zhang, W. Słysz, A. Pearlman, A. Verevkin and Roman Sobolewski, "Sensitivity and gigahertz counting performance of NbN superconducting single-photon detectors," *Appl. Phys. Lett.*, 84 , pp. 5338-5340, 2004.

[23] D. Rosenberg, A. E. Lita, A. J. Miller, and S. W. Nam, "Noise-free high-efficiency photon-number-resolving detectors," *Phys. Rev. A*, 71, pp. 061803-1-061801-4, 2005.

[24] A. J. Miller, S. W. Nam, J. M. Martinis, and A. V. Sergienko, "Demonstration of a low noise near-infrared photon counter with multiphoton discrimination," *Appl. Phys. Lett.*, 83, pp. 791-793, 2003.

[25] W. Du, H. Inokawa, H. Satoh, and A. Ono, "SOI metal-oxide-semiconductor field-effect transistor photon detector based on single-hole counting," *Opt. Lett.*, 36(15), pp. 2800-2802, 2011.

[26] W. Du, H. Inokawa, H. Satoh and A. Ono, "Single-Photon Detection by a Simple Silicon-on-Insulator Metal-Oxide-Semiconductor Field-Effect Transistor," *Jpn. J. Appl. Phys.*, 51(6), pp. 06FE01-1-06FE01-4, 2012.

Chapter 2

EFFECTS OF SUBSTRATE BIAS ON NOISE CHARACTERISTICS AND HOLE LIFETIME IN SOI METAL-OXIDE-SEMICONDUCTOR FIELD-EFFECT TRANSISTOR PHOTON DETECTOR

2.1 Introduction

A type of single-photon detector, which directly counts photo-generated and stored (or trapped) single charges by a sensitive electrometer, is drawing attention because of its potential as a photon-number-resolving detector [1-8]. Quantum dot field-effect transistor (QDFET) [2-4] utilizes the GaAs/AlGaAs two-dimensional electron gas (2DEG) channel as an electrometer to detect the photo-generated and trapped holes in the InAs self-organized QDs. Single-electron photodetector (photo-SET) [5,6] with nanocrystal silicon (nc-Si) dots formed by the deposition and annealing of Si-rich oxide utilizes single-electron transistor (SET) as an electrometer to detect photo-generated single charges trapped in the dot or Si/oxide interface. We have also

studied the scaled-down silicon-on-insulator (SOI) metal-oxide-semiconductor field-effect transistor (MOSFET) [7,8], in which photo-generated holes are stored below the negatively biased gate, and are detected as changes in the bottom-channel electron current. This SOI MOSFET is practically very attractive in that it can be manufactured by the standard Si integrated circuit technology and features small dark counts of $\sim 10^{-2}$ s^{-1} at room temperature, but issues remain such as low quantum efficiency (QE) and the slow operation speed [7], and this report intends to address the latter.

There are two main factors affecting the operation speed. One is the drain current noise. If the noise spectral density, the required signal-to-noise ratio for discriminating the current levels, and the charge sensitivity (change in the drain current) to a single hole are S_{Id} [A^2/Hz], SNR, and ΔI_d [A/hole], respectively, the maximum count rate can be roughly estimated as $(\Delta I_d/SNR)^2/S_{Id}$ [s^{-1}] indicating the low noise is required for high-speed operation. The other factor is the hole lifetime in the body of SOI MOSFET. In order to avoid the saturation of the number of stored holes at a high photon incident rate, short lifetime is desirable as long as the short output pulses can be resolved. In this report, we will describe the behavior of the drain current noise and the hole lifetime under different substrate voltages in search of optimum operation condition of the SOI MOSFET as a photon detector.

2.2 Device Structure

Although the original SOI MOSFET photon detector [7] had a special double-gate structure with a short lower gate (LG) and a long upper gate (UG) covering the p^--doped offset area between LG and n^+-doped source/drain, we select the ordinary n-channel fully-depleted (FD) SOI MOSFET without offset region [8] as shown in Fig. 1 considering its structural simplicity and versatility, and the device is fabricated in a 300-mm-wafer facility for Si integrated circuits to ensure the reproducibility.
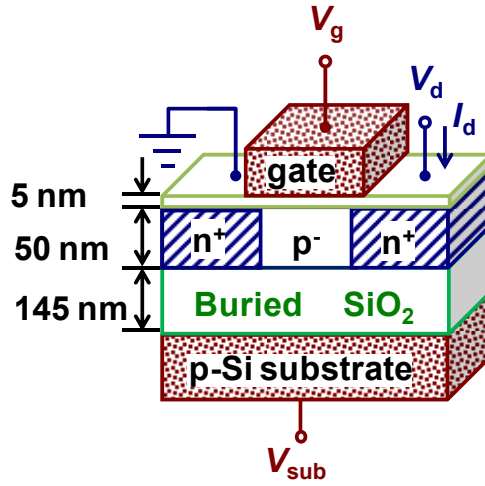
Figure 2-1 Schematic diagram of the SOI MOSFET. Thicknesses of buried oxide, SOI and gate oxide are 145, 50 and 5 nm, respectively.

It has n^+ poly-Si-gate and p^- channel region with dopant concentration less than 10^{15} cm^{-3}. The SOI is of a wafer-bonding type supplied by

Soitec S.A. [9]. Thicknesses of buried oxide, SOI and gate oxide are 145, 50 and 5 nm, respectively. The gate length is fixed at 300 nm, and the channel width is varied among 90, 95 and 110 nm. In the noise measurement and the hole lifetime analysis, we changed the substrate voltage V_{sub}, while keeping the drain current at the constant level of 1 nA by adjusting the front gate voltage V_g. The drain current noise was measured in dark condition at 300 K, and the hole lifetime was evaluated by the analysis of drain current histograms for different levels of light intensity also at 300 K.

2.3   Measurement Setup

2.3.1 Noise Measurement Setup

The block diagram of the noise measurement system is shown in Figure 3-2. For different V_{sub}, we analyzed the drain current noise through two differenct signal paths under dark condition at 300 K. For simple analysis, we recorded the source current waveform, which is equivalent to the drain one, using source measure unit (SMU) of the Agilent 4156C semiconductor parameter analyzer (SPA) with 0.1 s time step, and calculated the standard deviation. This will give the integrated noise in

the bandwidth of 5 Hz. For the detailed noise spectra in higher frequency range, we used HP35665A dynamic signal analyzer (DSA) combined with DL instruments model 1211 current preamplifier to attain input-referred noise (e.g. 2.5 fA/$\sqrt{Hz}$ for a sensitivity of 10^{-10} A/V) much smaller than the drain current noise.
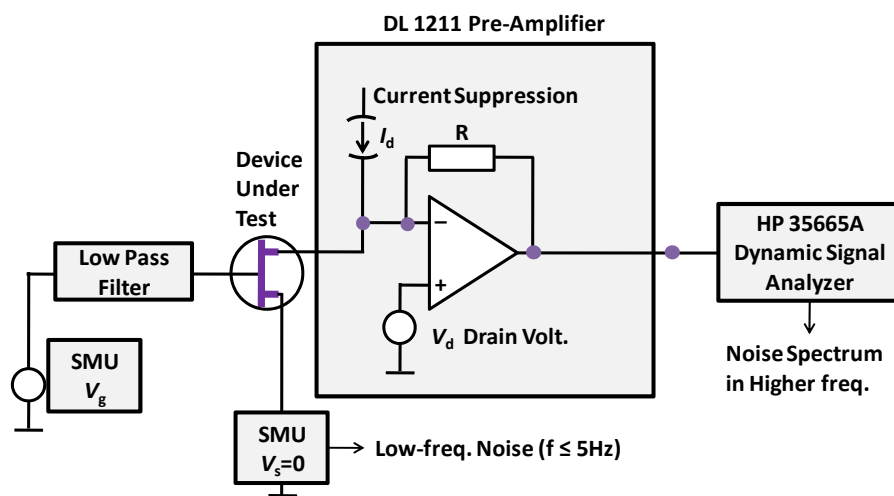
Figure 2-2 General block diagram of the measurement setup of noise measurement SOI MOSFET single-photon detector.

2.3.2 Hole Lifetime Measurement Setup

Figure 3-3 shown experiment setup in order to evaluate the hole lifetime, we used monochromatic light with a wavelength of 550 nm and analyzed the drain current waveforms under continuos light illumination with different intensites.
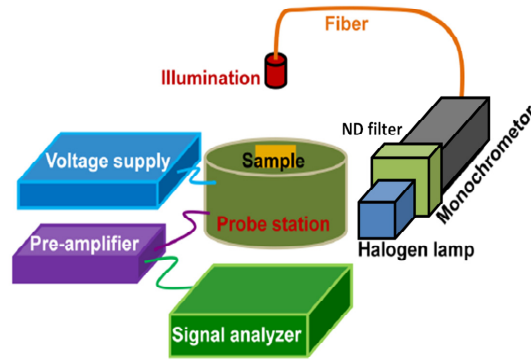
Figure 2-3 Schematic diagram of the measurement setup for the hole lifetime evaluation in SOI MOSFET photon detector.

The main measurement system utilized in this work consists of six (6) main blocks as shown in Figure 2-4.

1) Low-temperature prober Grail21-205-6-LV-R from Nagase Techno-Engineering Co., Ltd.

2) Compact monochromator H-20VIS from Horiba Jobin Yvon with halogen lamp as a light source.

3) Fiber optics for light guide.

4) Optical transfer system as an interface between light source and low-temperature prober.

5) Semiconductor parameter analyzer (SPA) 4156C from Agilent Technologies for DC electrical measurement and biasing.

6) DL1211 preamplifier and Signal Rocovery lock-in amplifier 7270 to record the drain current waveforms.
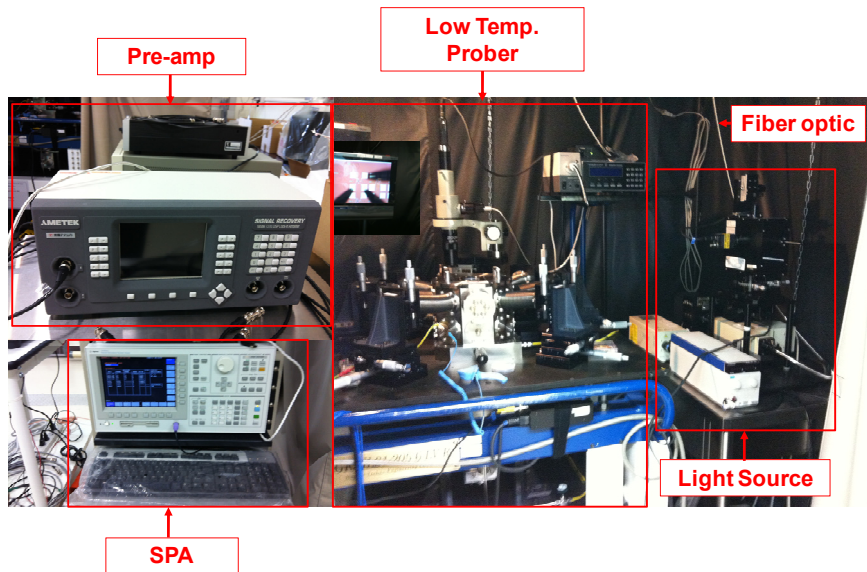
Figure 2-4 Measurement system consisting of a low-temperature prober, light source, semiconductor parameter analyzer (SPA), etc.

In this experiment, the sample temperature is kept at 300K, the prober chamber is evacuated by a turbo pump to 10^{-2} Pa. Temperature controller (Cryocon 32) is used to control the temperature.

The low-temperature prober with three main parts, as shown in Fig. 2-5, did not operate at low temperature in this experiment. The upper part is a measurement chamber with a sample stage and 6 probes connected a flange with triaxial connecters. From the connectoers, three or four triaxial cables, depending on the devices being measured, are connected to the semiconductor parameter analyzer. A Si diode is placed at the sample stage to sense the temperature and is connected to the temperature controller. The middle part is an area for the refrigerator driven by an external helium compressor.

In order to allow light illumination from outside, the upper part of the measurement chamber is equipped with a quartz glass window. This window also allows us to observe the sample by a digital microscope in order to precisely place the probes on the sample pads.
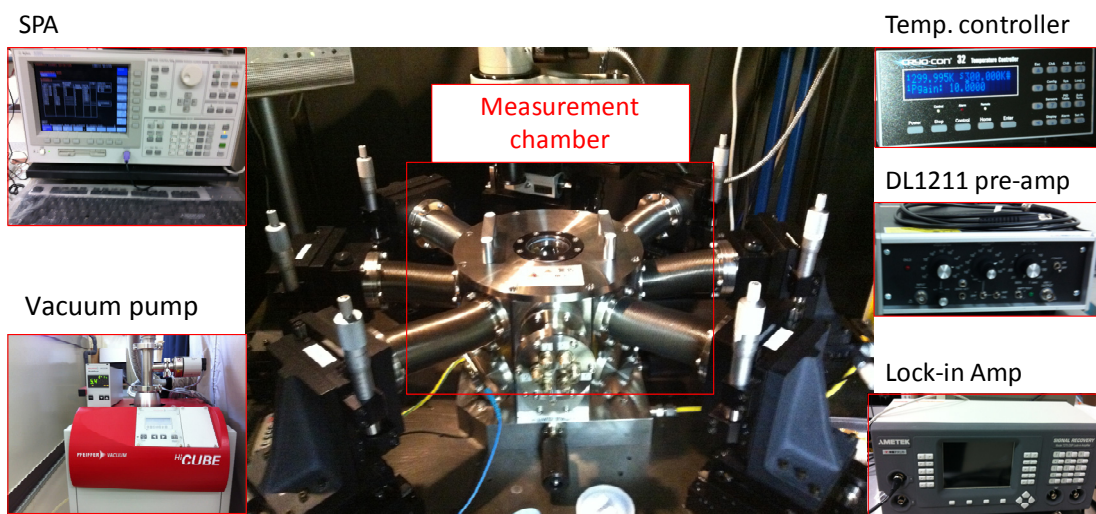
Figure 2-5 Low-temperature prober and the supporting systems.
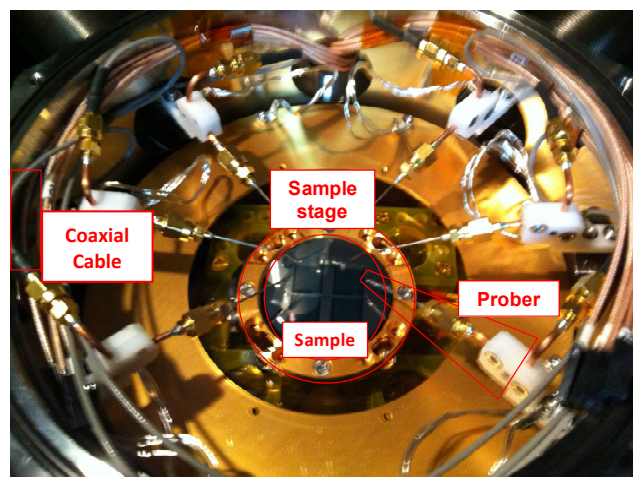
Figure 2-6 Sample on stage with six probes. The sample stage is used not only as the sample holder but also as a back gate terminal.

The device is placed on the sample stage in the measurement chamber as shown in Fig. 2-6. The sample stage is also used as a substrate (back gate) terminal. Through the quartz glass window, a monochromatic light in the visible wavelength is illuminated.

2.4   Experimental Result and Discussion

2.4.1 Analysis of Drain Current Noise

Figure 2-7 shows an example of I_d-V_g characteristics with V_{sub} as a parameter ranging from -10 to 10 V. Drain voltage V_d is kept at 50 mV. From these data, front-gate threshold voltage V_{th} corresponding to the I_d of 1 nA is extracted for setting the operation condition and further analysis. Figure 2-8 shows noise power for the bandwidth of 5 Hz, and the threshold voltage V_{th} plotted against the substrate voltage for various channel widths. In the V_{th}-V_{sub} characteristics, the deflection point 1 corresponds to the transition point between front- and back-channel operations, and the deflection point 2 to the transition between inversion and accumulation conditions at the buried oxide/substrate interface [10]. The noise levels show horseshoe shape, and become low at around the deflection point 1 and in the back-channel region between deflection

points 1 and 2. This behavior is common for three different channel widths W, although a slight inverse narrow-channel effect [11], i.e. the reduction of V_{th} for smaller W, can be seen.

Figure 2-9(a) shows the drain current noise spectra for front-channel operation. The drain current was kept at 1nA (substreshold operation), while the substrate voltage was varied from -10 to -3V. At V_{sub} = -3V the usual $1/f$ noise spectrum is observed, which can be explained by the McWhorter's model [12] based on the charge fluctuation in the slow oxide traps near the Si/oxide interface caused by the carrier tunneling to and from the inversion channel, and moreover includes the contributions of both front and back interfaces (coupling effects) in the present case of FD SOI MOSFET [13].

As the V_{sub} decreased, an excess Lorentzian noise begin to evolve at V_{sub} = -5V which corresponds to a weakly accumulated back interface, when the magnitude of V_{sub} increases the noise spectra asymptotically approach a single $1/f^2$ line, indicating that the Lorentzian plateau level and time constant increase simultaneously. Figure 2-9(b) shows the noise spectra for back-channel operation in $-3 \leq V_{sub} \leq 4V$. The similar behavior of the evolution of the noise spectra can be observed, when the front interface is driven toward accumulation.
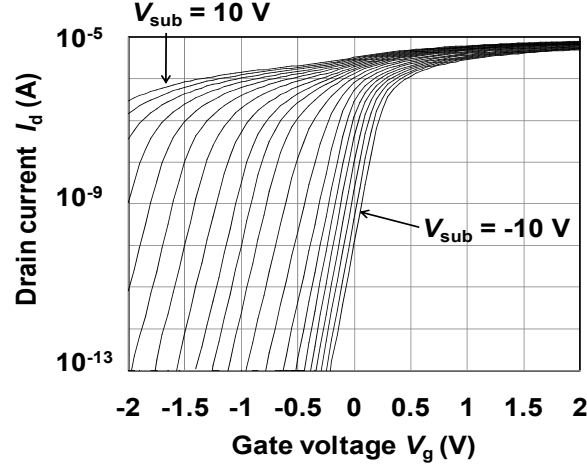
Figure 2-7 I_d-V_g characteristics with V_{sub} as a parameter. Drain voltage V_d is kept at 50 mV. Device sizes are L= 300 nm and W= 110 nm.
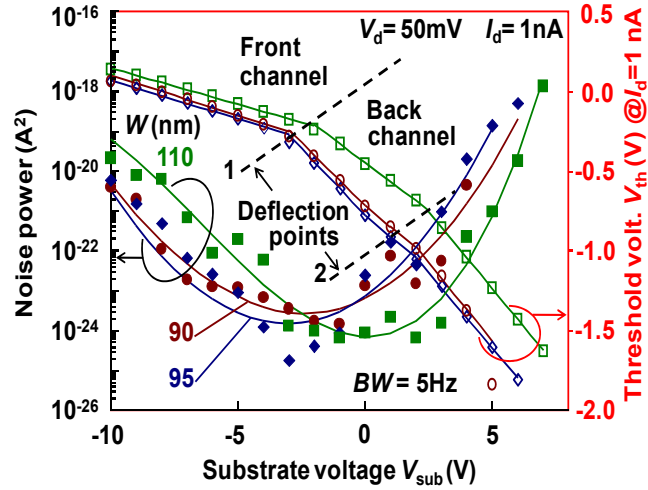
Figure 2-8 Noise power and front-gate threshold voltage V_{th} at 1 nA as a function V_{sub}. The gate length is fixed at 300 nm, channel width is varied among 90, 95 and 110 nm.
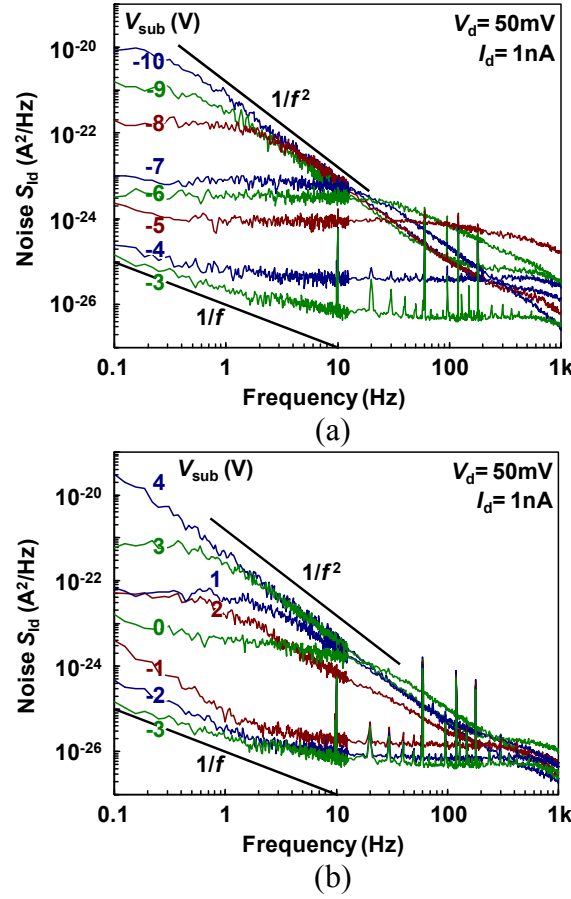
Figure 2-9 Drain current noise spectra for (a) front-channel ($-10 \leq V_{sub} \leq -3$V), and (b) back-channel ($-3 \leq V_{sub} \leq 4$V) operations. Device sizes are $L= 300$ nm and $W= 95$ nm.

In SOI MOSFET, the Lorentzian excess noises are often associated with the body potential fluctuation caused by several mechanisms of majority carrier generation [13-15], such as (a) impact ionization, (b) gate-induced drain leakage (GIDL) and other drain-body junction leakage, (c) tunneling through a thin gate oxide, (d) tunneling between back-gate-induced (BGI) accumulation layer and source/drain region, etc. However, these floating-body (FB) induced excess noises are not likely in the present device primary due to its FD operation, in which lower potential

barrier at the source/body junction alleviates the accumulation of the majority carriers. In addition, low drain voltage of 50 mV, nearly symmetric behavior of the noise with respect to V_{sub}, and thick gate oxide of 5 nm are also incompatible with the mechanisms (a), (b), and (c), respectively. BGI Lorentzian noise (d) was actually reported in FD SOI MOSFET [16], but the Lorentzian time constant decreased as $|V_{sub}|$ increased, which contradicts the behavior observed in the present experiment. Apart from the above FB mechanisms, D. S. Ang, et al. reported the very similar evolution of the noise spectra in the transition from FD to near FD operation, caused by the generation-recombination (GR) processes at bulk defects in the depleted SOI layer [17]. In our device, as can be seen in Fig. 4 (a) and (b), the asymptotic $1/f^2$ lines for both negative and positive V_{sub}, i.e. front- and back-channel operations, are quantitatively the same. This symmetric behavior strongly suggests the origin of the GR noise in the present device is not located at the front or back interface, but in the depleted SOI layer. This observation also excludes the possibility of random telegraph signal (RTS) [18], which is caused by the charge fluctuation in a single oxide trap and possibly shows the Lorentzian spectrum, because the individuality of the oxide traps in energy level and location in the oxide cannot lead to the common noise spectrum for both front- and back-channel operations.

For understanding the behavior of Lorentzian (GR) noise, we try to model the Lorentzian noise base on equation 2.1. [12]

$$S(f) \propto \frac{A\tau}{1 + (2\pi f \tau)^2}$$
(2.1)

where A is amplitude of Lorentzian noise and τ is recombination lifetime. By keeping ratio of the amplitude A and recombination lifetime τ constant as shown in Table 2.1, noise spectra asymptotically approach a single $1/f^2$ line as shown in Figure 2-10, indicating that the active trap density and carrier lifetime increased simultaneously.

Table 2.1 Paramaters for Lorentzian model

Case	A (A²)	τ (s)	A/τ (A²/s)
1	2×10^{-20}	1×10^{0}	2×10^{20}
2	1.25×10^{-21}	6.25×10^{-2}	2×10^{20}
3	7.81×10^{-23}	3.91×10^{-3}	2×10^{20}
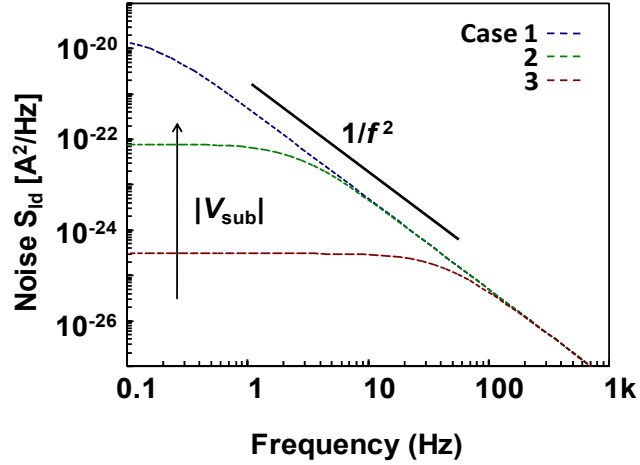
Figure 2-10 Behavorial model of Lorentzian (GR) noise. Ratio of the amplitude A and recombination lifetime τ are kept in constant value.

(a)   (b)
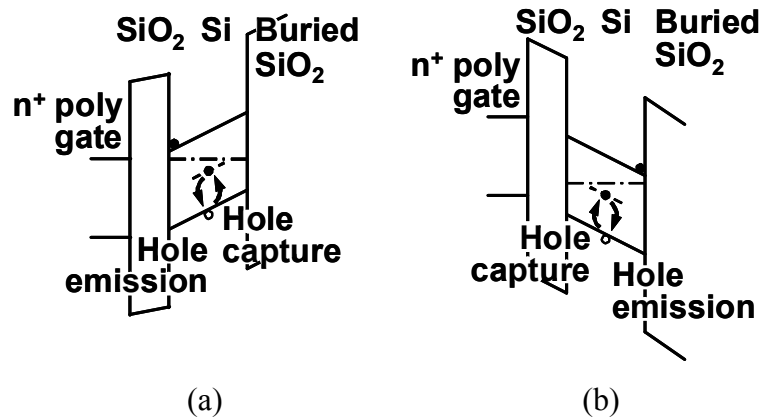
Figure 2-11 Lorentzian noise mechanism for (a) front-channel operation with $V_{sub}<0$, $V_g\sim0$, and (b) back-chanel operation with $V_{sub}>0$, $V_g<0$.

Figure 2-11 shows the Lorentzian (GR) noise mechanism, in which, at higher electric field, the traps in wider energy range contribute to the hole emission (field-assisted emission), and hole capture rate decreases due to the localization of holes.

2.4.2 Analysis of Hole Lifetime

Figure 2-12 shows typical drain current waveforms for different levels of light intensity at the wavelength of 550 nm. Baseline current is adjusted to 1 nA by V_g, and each waveform is shifted for clarity. V_d and V_{sub}, are 0.05 and 1.49 V, respectively. In this figure, we can see that the photo-generated holes modulate the drain current to discrete levels corresponding to the number of stored holes below the gate n_h, while the operating condition is set to $V_g < 0$ and $V_{sub} > 0$, so that the electrons flow in the back-channel. Note that, in dark condition, we could not observe signal exceeding the level of $n_h = 1$, or RTS-like behavior. Actually, the randomness in the waveforms of Fig. 5 is caused by the statistical fluctuation of the photon arrival (hole generation) and hole recombination, which follow the Poisson process.

As described in [7], the evolution of the state probability corresponding to each n_h can be explained well by the rate equation taking the hole generation and recombination rates into account, and this is the basis of the hole lifetime analysis.
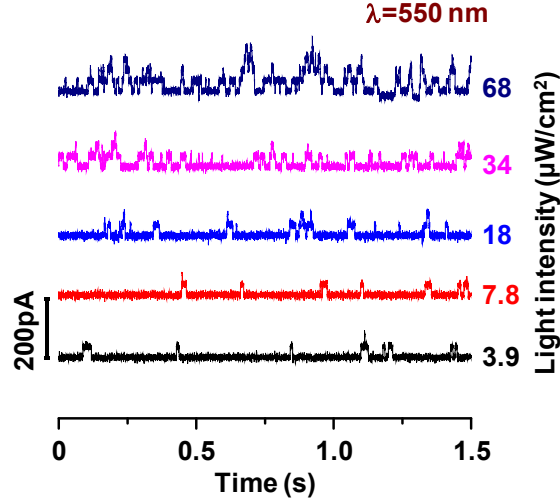
Figure 2-12 Typical drain current waveforms at 300 K for different levels of light intensity at the wavelength of 550 nm. Baseline current is adjusted to 1 nA by V_g, and each waveform is shifted for clarity. V_d and V_{sub} are 0.05 and 1.49 V, respectively. Device sizes are L= 300 nm and W= 110 nm.

Figure 2-13 shows the histograms of drain current for (a) V_{sub}= 1.27 V, (b) V_{sub}= 1.49 V, (c) V_{sub}= 1.72 V, and (d) V_{sub}= 1.93 V with different V_g to keep the baseline drain current at the same level of 1 nA. The closed symbols are obtained data and solid lines are fitting curves with Gaussian distribution. The peaks from left to right correspond to the number of stored holes of 0, 1, 2 and 3. It can be seen that the peaks in the histogram corresponding to the larger number of stored holes become higher as the V_{sub} increases. This may be caused by the longer hole lifetime, higher light absorption efficiency or higher collection efficiency of the photo-generated holes.
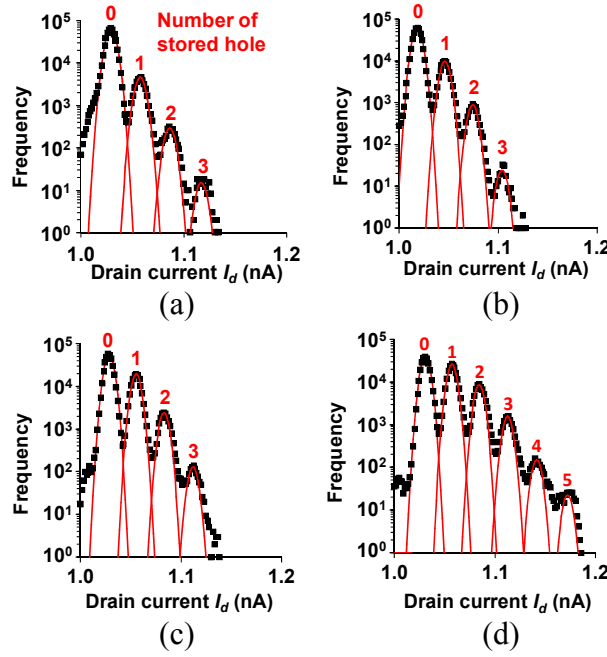
Figure 2-13 Histograms of drain current for (a) V_{sub}= 1.27 V, (b) V_{sub}= 1.49 V, (c) V_{sub}= 1.72 V, and (d) V_{sub}= 1.93 V with different V_{sub} to keep the baseline drain current at the same level of 1 nA under the continuous light illumination of 34 μW/cm^2. The first, second, third, and fourth peaks correspond to the number stored holes of 0, 1, 2 and 3, respectively. Data acquisition time period and time step are 2.45 s and 49 μs, respectively, and 50000 (= 2.45 s / 49 μs) data points (current values) are classified into bins with a width of 2 pA. Device sizes are L= 300 nm and W= 110 nm.

In order to understand the bias dependence of the light absorption and hole collection, hole generation rate is plotted against the light intensity in Fig. 2-14. There is proportionality between hole generation rate and incident light intensity regardless of V_{sub}, indicating that light absorption or hole collection efficiencies is not much changed by the bias condition. This also means that the hole lifetime can be controlled

without affecting the nominal QE (as defined by the fraction of photons entering the detection area that are counted), which amounts to 0.15% in this case assuming the detection area of 300×110 nm^2.

The hole lifetimes are obtained as fitting parameters to describe the evolution of drain current histogram based on the rate equation under steady state conditions, $f_i / \tau_i = f_{i-1} R$ and $\Sigma f_i = 1$, where τ_i and f_i are hole lifetime and probability of state corresponding to hole number i, and R is hole generation rate [7]. The hole lifetimes at different V_{sub} are depicted in Fig. 2-15. It can be seen the hole lifetime increases significantly as V_{sub} increases. It is estimated that higher V_{sub} (higher transverse electric field) separates the stored hole and electron more effectively, and reduces the probability of recombination, leading to the longer lifetime.
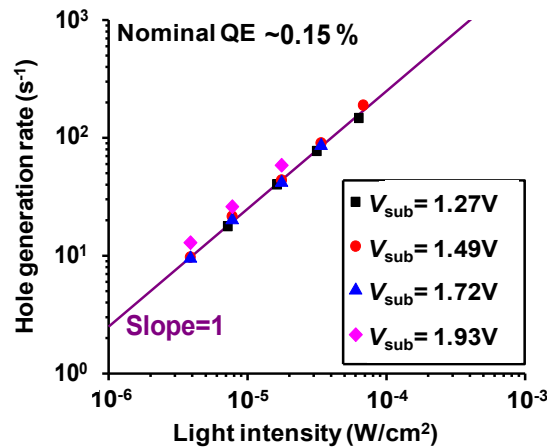
Figure 2-14 Hole generation rate as a function of incident light intensity for each bias condition. Slope of the fitting line is one.
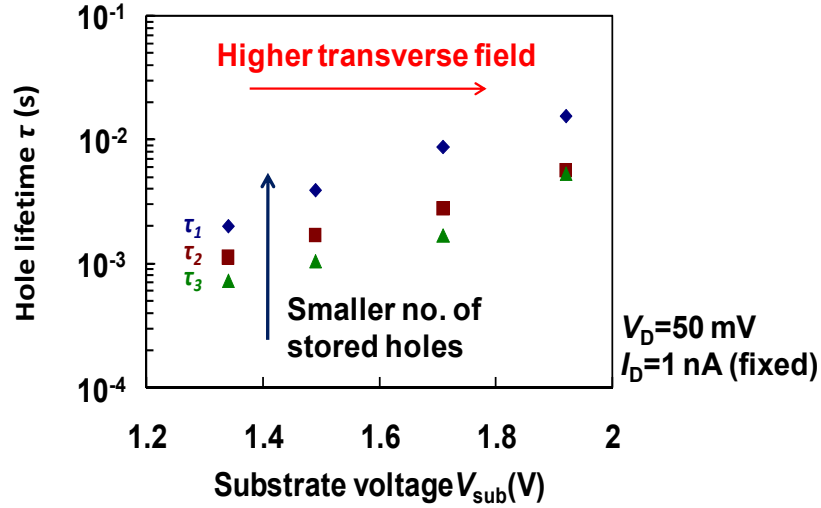
Figure 2-15 Hole lifetime as a function of V_{sub}. τ_1, τ_2 and τ_3 are the lifetimes when the number of the stored holes are one, two and three, respectively.

In case of QDFET, the hole lifetime in InAs QDs is longer than a hundred seconds, and a reset gate pulse is necessary for refilling the dots with electrons after illumination [3,4]. In the photo-SET, electron lifetime in the nc-Si dots (detection time) can be as long as 350 s at a specific temperature with the contribution of Si/oxide traps [6]. In the present SOI MOSFET, hole lifetime is much shorter probably due to the bulk defects in the SOI layer as estimated in the previous section, the presence of channel electrons in a short distance, and the lose confinement of holes in the shallow potential well created by the pn junction and gate electric field. The short lifetime is beneficial in that the device does not require reset operation, but there might be some difficulty in controlling the lifetime to an appropriate value. The contribution of the Si/oxide interface traps [6] to the hole lifetime seems to be small considering the fact that

the lifetime becomes longer for higher transverse electric field that makes the hole distribution closer to the interface.

It is worthwhile to compare other performance indices of the QDFET and SOI MOSFET. The QE of QDFET is reported to be 0.14% [3] and comparable to 0.15% of the present SOI MOSFET. There are common issues in the small light absorption in thin active layer, and low transmittance of the metallic gate. Higher QE may be attained by the introduction of a resonant cavity structure and more transparent gate material. The dark count rate in the SOI MOSFET is less than 0.2 s^{-1} (no signal in the observation time of 5 s) at 300 K, and this outperforms the 10^{-8} ns^{-1} of the QDFET at 77 K [3], indication the SOI MOSFET is suitable to applications where the photon arrival time is not known.

2.5   Operation Speed

Operation speed of the single-photon detection, i.e. maximum count rate, is limited by the noise and the hole lifetime as described in the Introduction. According to the results in Sections 2.3 and 2.4, the small $|V_{sub}|$ leads to high-speed operation owing to the low noise and short lifetime. It can be seen in Fig. 2-8 that the minimum noise power for the band width of 5 Hz is 7×10^{-25} A^2 (S_{Id} is 1.4×10^{-25} A^2/Hz). ΔI_d is found

to be 29 pA as the peak-to-peak spacing in Fig. 2-13. If we assume the required SNR of 10 dB (=3.16), the maximum count rate $(\Delta I_d / SNR)^2 / S_{Id}$ becomes 600 s^{-1}. Figure 8 also indicates that the minimum hole lifetime τ_l of 2×10^{-3} s makes the maximum count rate to be about 500 s^{-1} ($=1/\tau_l$) to avoid the excessive accumulation of holes. In order to improve these values, ΔI_d could be increased by further down-scaling of the device sizes, and τ_l could be reduced by introducing defects.

Conclusion

Substrate bias dependence of the drain current noise and hole lifetime in SOI MOSFET is evaluated *for the first time* in relationship to photon detector performance. Low-frequency current noise in SOI MOSFET was analyzed for photon detection under different V_{sub}'s. It was found that the noise in the SOI MOSFET became low at the transition point between the front- and back-channel operations, and in the back-channel region near the transition point. On both sides, the noise spectra asymptotically approached a single $1/f^2$ line, indicating that the Lorentzian plateau level and time constant increase simultaneously presumably due to the GR processes at bulk defects in the SOI layer. In order to understand the V_{sub} dependence of the hole lifetime, the drain current histograms of the SOI MOSFET were analyzed at different V_{sub}'s and light intensities. It was found that the peaks in the histogram corresponding to the larger number of stored holes became higher as the V_{sub} decreased. This was attributed to the prolonged hole lifetimes caused by the higher electric field inside the body of SOI MOSFET. It can be concluded that, once the inversion channel is induced for detection of the photo-generated holes, the small $|V_{sub}|$ is favorable for short lifetime and low noise, leading to high-speed operation.

References

[1] R. P. Mirin, S. W. Nam, and M. A. Itzler, "Single-Photon and Photon-Number-Resolving Detectors," *IEEE Photonics J.* **4**(2), 629-632 (2012).

[2] B. E. Kardynal, S. S. Hees, A. J. Shields, C. Nicoll, I. Farrer, and D. A. Ritchie, " Photon number resolving detector based on a quantum dot field effect transistor," *Appl. Phys. Lett.* **90**(18), 181114 (2007).

[3] B. E. Kardynal, A. J. Shields, N. S. Beattie, I. Farrer, K. Cooper, and D. A. Ritchie, "Low-Noise Photon Counting with a Radio-Frequency Quantum-Dot Field-Effect Transistor," *Appl. Phys. Lett.* **84**(3), 419–421 (2004).

[4] A. J. Shields, M. P. O'sullivan, I. Farrer, D. A. Ritchie, M. L. Leadbeater, N. K. Patel, R. A. Hogg, C. E. Norman, N. J. Curson, and M. Pepper, "Single Photon Detection with a Quantum Dot Transistor," *Jpn. J. Appl. Phys.* **40**(3B), 2058-2064 (2001).

[5] M. Troudi, N. Sghaier, A. Kalboussi, and A. Souifi, "Analysis of photogenerated random telegraph signal in single electron detector (photo-SET)," *Opt. Lett.* **18**(1), 1-9 (2010).

[6] S. Chatbouri, M. Troudi, N. Sghaier, V. Aimez, D. Drouin, and A. Souifi, "Traps contribution on detection time of single electron

photodetector (Photo-SET)," *Semicond. Sci. Technol.* **29**, 085003 (2014).

[7] W. Du, H. Inokawa, H. Satoh, and A. Ono, "SOI metal-oxide-semiconductor field-effect transistor photon detector based on single-hole counting," *Opt. Lett.* **36**(15), 2800-2802 (2011).

[8] W. Du, H. Inokawa, H. Satoh, and A. Ono, "Single-Photon Detection by a Simple Silicon-on-Insulator Metal-Oxide-Semiconductor Field-Effect Transistor," *Jpn. J. Appl. Phys.* **51**(6), 06FE01(2012).

[9] Soitec S.A., Parc Technologique des Fontaines, 38190 Bernin, France.

[10] S. Horiguchi, A. Fujiwara, H. Inokawa, and Y. Takahashi, "Analysis of back-gate voltage dependence of threshold voltage of thin silicon-on insulator metal-oxide-semiconductor field-effect transistor and its application to Si single-electron transistor," *Jpn. J. Appl. Phys.* **43**(4B), 2036-2040 (2004).

[11] N. Shigyo and T. Hiraoka, "A review of narrow-channel effects for STI MOSFET's: A difference between surface- and buried-channel cases," *Solid-State Electronics* **43**(11), 2061-2066 (1999).

[12] A. L. McWhorter, "1/f noise and germanium surface properties," in Semicond. Surf. Phys, R. H. Kingston, ed., (University of Pennsylvania Press, 1957) p. 207.

[13] E. Simoen, A. Mercha, C. Claeys, and N. Lukyanchikova, "Low-frequency noise in silicon-on-insulator devices and technologies," Solid-State Electronics **51**(1), 16-37 (2007).

[14] G. O. Workman and J. G. Fossum, "Physical Noise Modeling of SOI MOSFET's with Analysis of the Lorentzian Component in the Low-Frequency Noise Spectrum," *IEEE Trans. Electron Devices* **47**(6), 1192-1201 (2000).

[15] Y.-C. Tseng, W. M. Huang, M. Mendicino, D. J. Monk, P. J. Welch, and J. C. S. Woo, "Comprehensive Study on Low-Frequency Noise Characteristics in Surface Channel SOI CMOSFETs and Device Design Optimization for RF ICs," *IEEE Trans. Electron Devices* **48**(7), 1428-1437 (2001).

[16] N. Lukyanchikova, N. Garbar, A. Smolanka, M. Lokshin, E. Simoen, and C. Claeys, "Origin of the front-back-gate coupling in partially depleted and fully depleted silicon-on-insulator metal-oxide-semiconductor field-effect transistors with accumulated back gate," *J. Appl. Phys.* **98**(11), 114506 (2005).

[17] D. S. Ang, Z. Lun, and C. H. Ling, "Generation-recombination noise in the near fully depleted SIMOX N-MOSFET operating in the linear region," *IEEE Trans. Electron Dev.* **50**(12), 2490-2498 (2003).

[18] Z. Shi, J. P. Mieville, and M. Dutoit, "Random telegraph signals in deep submicron n-MOSFET's," *IEEE Trans. Electron. Dev.* **41**(7), 1161-1168 (1994).

PERFORMANCE ESTIMATION OF SOI MOSFET PHOTON DETECTOR

In the previous chapter, we evaluated the effect of substrate voltage on the noise and hole lifetime in the SOI MOSFET photon detector for better operation speed, but the improvement is limited by the MOSFET under investigation. In this chapter, we estimate the attainable performance of the photon detector based on single-charge counting, and make clear the requirement to achieve the target performance in terms of dark count and maximum count rates.

3.1 Introduction

A scaled-down Silicon on insulator (SOI) metal-oxide-semiconductor field effect transistor (MOSFET) with gate length $L=65$ nm and channel width $W=105$ nm has been found to operate as a single-photon detector [1-2], which features very small dark count (~ 0.01 s^{-1}) at room temperature, low operation voltage (~ 1 V), and photon-number resolution. In this chapter, we will estimate the attainable performance,

based on the newly developed model of the output waveforms and the signal-processing algorithm.

In the SOI MOSFET with a special double-gate structure, a short lower gate (LG) and a long upper gate (UG) covering the entire p⁻-doped SOI area was used to create potential well below the LG to store photo-generated holes, as shown in Fig. 3-1, photogenerated holes are stored below the negatively biased gate, and the presence of the holes is detected as the change in electron current flowing through the inversion layer induced by the positive back-gate (substrate) voltage.

Figure 3-2 shows typical drain current waveform at dark and under illumination light with wavelength 550 nm at room temperature. Baseline is shift for clarity, as we can see photogenerated holes modulate drain current as increasing light intensity.
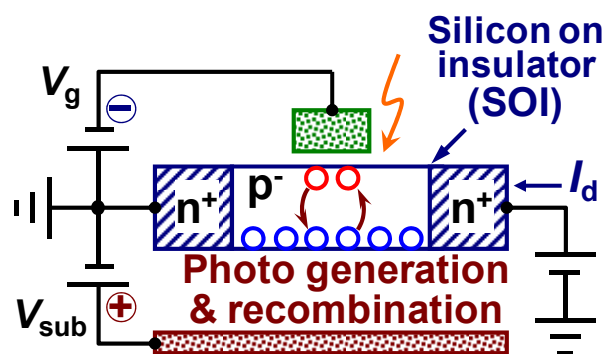
Figure 3-1 Schematic diagram of the SOI MOSFET single-photon detector.
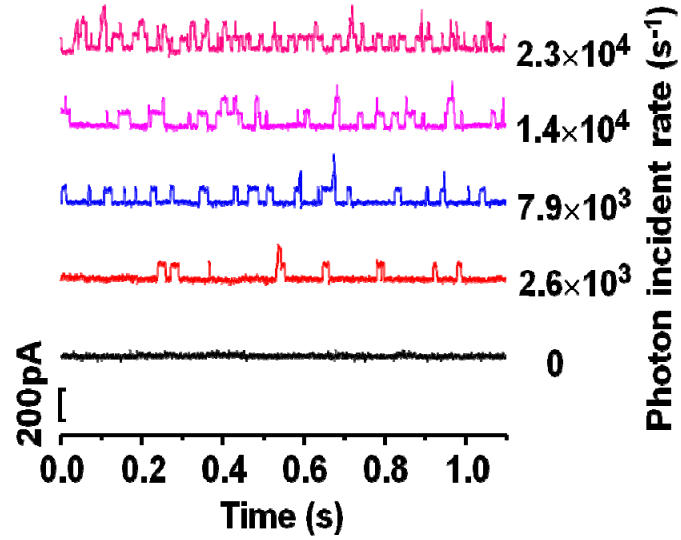
Figure 3-2 I_D waveforms at 300 K for various light intensities (λ=550 nm). Base line current is about 1 nA, and each waveform is shifted for clarity.

3.2 Simulation Results and Discussion

3.2.1 Simulation method for output signal generation

The fluctuation of drain current waveform cause by photo-generation and recombination of holes in the body of SOI MOSFET are simulated as independent Poisson processes [3], whose timings are set by random numbers based on equation T_i= -ln(r_i)/R, where r_i is a random number distributed uniformly between 0 and 1. [4]

The basic equation of Poisson distribution for probability that a certain event takes place k times in a unit time is expressed by

$$P(N= k)= \frac{e^{-\lambda}\,\lambda^k}{k!} \tag{3.1}$$

when the average event number is λ. Here, k is a natural number including zero, $k!$ is the factorial of k, and λ is a positive real number. For example, the probability to receive k photons in an observation time T is given by equation 3.1 with $\lambda=RT$, where R is the incident rate [1/s] of photons.

Another basic equation of the Poisson process for probability that a certain event takes place k times before time t is expressed by

$$P(N_t= k)= \frac{e^{-\lambda t}\,(\lambda t)^k}{k!} \tag{3.2}$$

where λ is average event number in a unit time, and N_t is number of event took place before the time t. Especially, if zero is substituted for k, $P(N_t= 0)$ becomes the probability that waiting time T before an event is longer than t is given by

$$P(T> t)= P(N_t= 0) = \exp(-\lambda t) \tag{3.3}$$

For example, If the recombination rate of hole and electron is R [1/s], the probability that the waiting time T before the recombination is longer than t is

$$P(T>t)=\exp(-Rt) \tag{3.4}$$

The simulation is based on the flowchart of generation and recombination events in the detector as shown in Fig. 3-3. It can be understood from the flowchart that the number of hole increases if the

waiting time before hole generation is smaller than waiting time before hole recombination, while the number of hole decreases if the waiting time before hole generation is larger than waiting time before hole recombination. After that the time proceeds by the waiting time, and the same steps of hole generation/recombination event is repeated until the total number of events is reached.

Uniform random numbers
r_g, r_r between 0 & 1

Wait time before hole generation* $T_g = -\dfrac{\ln(r_g)}{R_g}$

Wait time before hole recombi.* $T_r = -\dfrac{\ln(r_r)}{R_r}$

yes — $T_g < T_r$ — no

Hole generation
$n_h = n_h + 1$
$t_{n+1} = t_n + T_g$

Hole recombi.
$n_h = n_h - 1$
$t_{n+1} = t_n + T_r$

n_h: number of stored holes (≥ 0)
R_g: hole generation rate by light
R_r: hole recombination rate
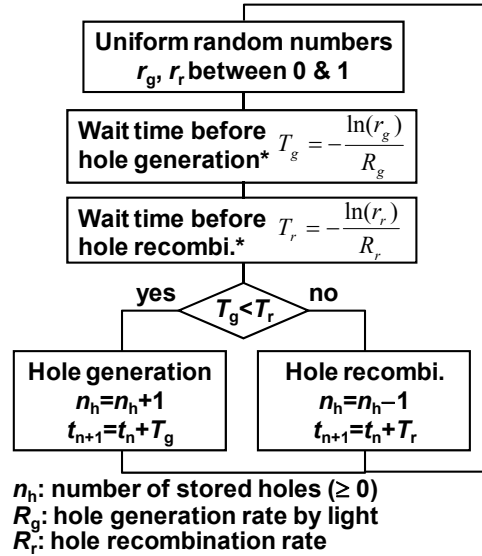
Figure 3-3 Flowchart of the output signal simulation for SOI MOSFET single-photon detector.

3.2.2 Generation of Detector Output

The dark red line in Fig. 3-4 is a typical simulation result of detector output for hole generation and recombination rate of 5 x 10^4 s^{-1} and sampling frequency of 1 MHz. To this output, noise of normal

random number with standard deviation of 0.1 e is added as shown in the dark blue line of Fig. 3-4.

In order to detect the events of hole generation by photon incidence and recombination, the output signal is differentiated, and positive and negative peaks are associated respectively with the hole generation and recombination events as shown in Fig. 3-5. The differentiation used in this simulation is based on the 1st derivative operation using quadratic function fitted to 3 data points. As we can see from the figure, the differentiation makes the processing insensitive to baseline shift, and the integration makes immune to the noise.
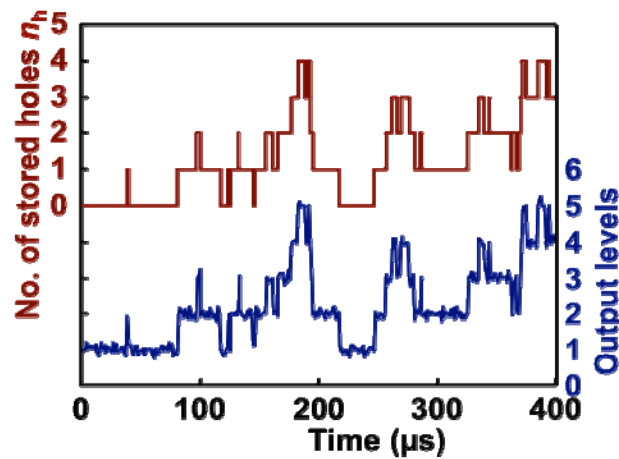
Figure 3-4 Simulated time sequence of the number of stored holes in the SOI MOSFET. Detector output signal is generated by adding of normal random number.
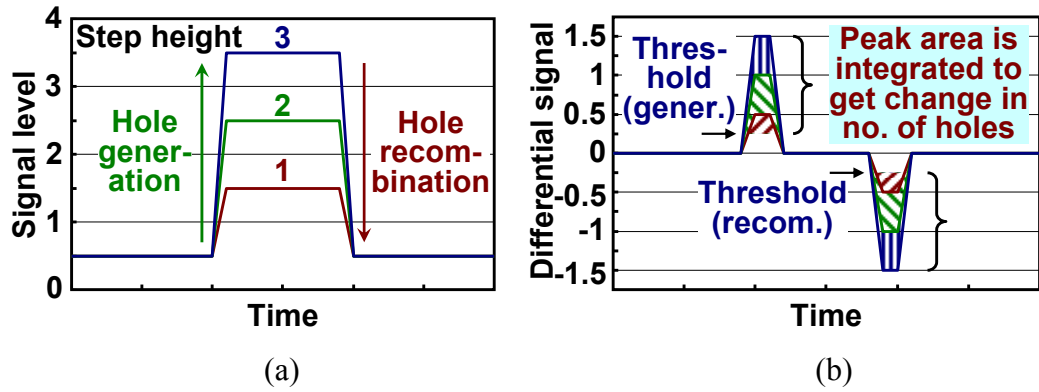
Figure 3-5 Schematics to show the signal processing algorithm to detect the hole generation and recombination events. (a) Detector output signal as function of time, and (b) differentiated signal to judge the numbers of generated or recombined holes.
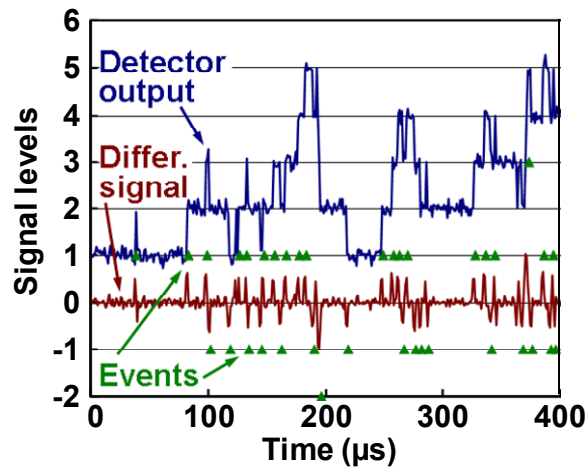
Figure 3-6 Simulated output signal, differentiated signal, and the detected events of hole photo-generation and recombination.

Number of stored holes is correlated to the discrete levels of the detector output as is seen in Fig. 3-6. The output levels are kept until recombination takes place. Positive and negative values of events (triangles in Fig. 3-6) correspond to generation and recombination, respectively, and the absolute value indicates the number of holes

involved in the event, i.e. multiple holes are generated or recombined at one time in some cases.

3.2.3 *Maximum Count Rate*

Based on the linearity between detected and generated rates of holes, and detected rate under null generation for different noise levels and sampling frequencies, correlation between maximum and dark count rates is established. We can define the maximum count rate of the sampled signal by 10% deviation from the linear relationship of the count and hole generation rates as shown in Figure 3.7. Maximum count rate for 10% count error corresponds to 1/20 of sampling frequency (f_s). The expression for the maximum count rate (MCR) = <u>0.05</u> x f_s, where the underlined value 0.05 is a parameter that depends on signal processing algorithm.
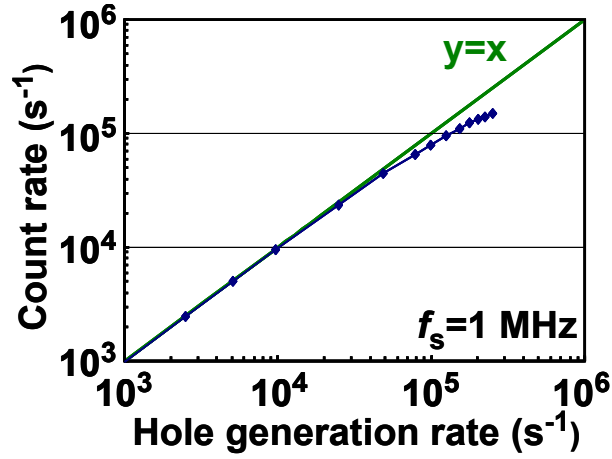
(a)
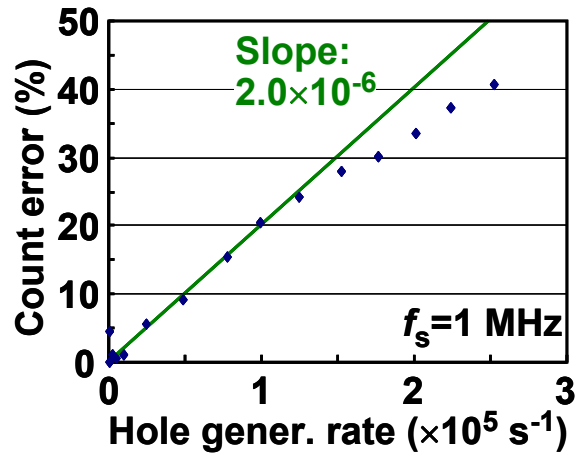
(b)

Figure 3-7 (a) Count rate as a function of hole generation rate, and (b) count error as a function of hole generation rate.

3.2.4 Dark Count Rate

The dark count rate is determined from the simulation result of photo-generation and recombination of holes for different standard deviations of noise and sampling frequency of 1 MHz. As we can see in Figure 3-8 the relationship between dark count rate and noise is described well by cumulative normal distribution, i.e. it can be express by

DCR=$\underline{0.67}\times f_s \times F(1,\underline{1.81}\times\sigma_n)$, where f_s in sampling frequency, the underlined values are parameters that depend on signal processing algorithm, and $F(x, \sigma)$ is cumulative normal distribution expressed by

$$F(x,\sigma) = \int_x^\infty \frac{1}{\sqrt{2\pi}\sigma}\exp\left(-\frac{x^2}{2\sigma^2}\right)dx \qquad (3.4)$$

While the standard deviation of noise σ is correlated to charge sensitivity δQ (e/$\sqrt{Hz}$) (figure merit of charge detector), it can be formulated by

$$\sigma_n = \delta Q \times \sqrt{f_s}/2 . \qquad (3.5)$$
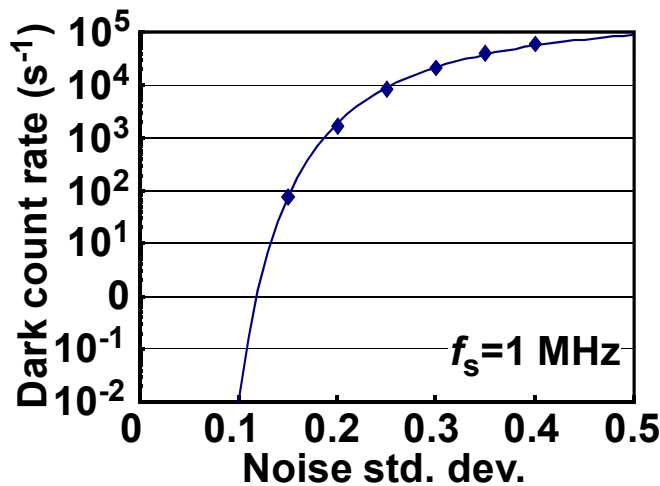
Figure 3-8 Dark count rate as a function of noise standard deviation.

The estimated performance of the single-photon detector based on single-charge counting is shown in Figure 3-9. A record-high dynamic range 178 dB (maximum and dark count rates of 7.6 Ms^{-1} and 0.01 s^{-1}, respectively) can be attained by a state-of-the-art charge sensor with

charge (hole) sensitivity of 1×10^{-5} e/$\sqrt{\text{Hz}}$ [5] and sampling frequency of 150 MHz.
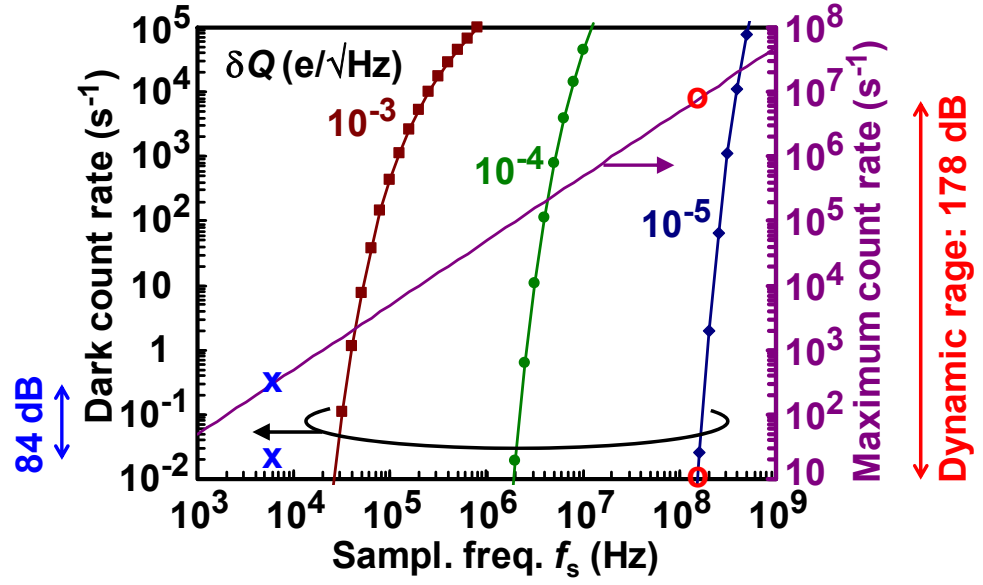
Figure 3-9 Dark count and maximum count rates as a function of sampling frequency for various charge sensitivity δQ (e/$\sqrt{\text{Hz}}$). **x** and **o** correspond to the performance of the present detector and the hypothetical one with a state-of-the-art charge sensor, respectively.

Conclusion

In conclusion, dark and maximum count rates are quantitatively correlated to the sensitivity of the single-charge detector *for the first time* considering the application to single-photon detector. The attainable performance of the single-photon detector based on single-charge counting is estimated by the newly-developed simulation method of detector output and signal processing algorithm. The photon detector with a state-of-the-art charge sensor can realize the maximum count rate of 7.6 Ms^{-1}, the dark count rate of 0.01 s^{-1}, and the resultant dynamic range of 178 dB, which is 70 dB higher than that of conventional APD, and 90 dB higher than that of the current SOI MOSFET. In order to attain such high performance, the charge sensitivity of the SOI MOSFET should be further improved to the level of 10^{-5} e/√Hz.

References

[1]   W. Du, H. Inokawa, H. Satoh, and A. Ono, " SOI metal-oxide-semiconductor field-effect transistor photon detector based on single-hole counting," *Opt. Lett.* 36(15), pp. 2800-2802, 2011.

[2]   W. Du, H. Inokawa, H. Satoh, and A. Ono, "Single-Photon Detection by a Simple Silicon-on-Insulator Metal-Oxide-Semiconductor Field-Effect Transistor," *Jpn. J. Appl. Phys.*, 51(6), pp. 06FE01-1-06FE01-4, 2012.

[3]   G.E. Johnson, "Constructions of particular random processes," *Proc. IEEE* 82, 270, 1994.

[4]   M. Kirihara, N. Kuwamura, K. Taniguchi, and C. Hamaguchi, "Monte Carlo Study of Single-Electronic Devices," *Proc. SSDM*, pp. 328-330, 1994.

[5]   R. J. Schoelkopf, P. Wahlgren, A. A. Kozhevnikov, P. Delsing, D. E. Prober, "The Radio-Frequency Single-Electron Transistor (RF-SET): A Fast and Ultrasensitive Electrometer," *Science*, 280, pp. 1238-1242, 1998.

SINGLE-PHOTON DETECTION BY A SILICON ON INSULATOR FIN-TYPE FIELD-EFFECT TRANSISTORS

In the previous chapter, we quantitatively estimated the potential performance of SOI MOSFET photon detector in terms of dark count and maximum count rates, and concluded that the charge sensitivity in the order of 10^{-5} e/$\sqrt{Hz}$ is necessary to outperform the conventional detectors. In this chapter, we investigate the photoresponse of the silicon-on-insulator (SOI) fin-type field-effect transistor (FinFET), which has a better scalability and is expected to give higher charge sensitivity and improved performance as a photon detector.

4.1 Introduction

The silicon on insulator (SOI) metal-oxide-semiconductor field-effect transistor (MOSFET) can operate as a single-photon detector, featuring dark counts several orders of magnitude smaller than that of

conventional avalanche photodiode (APD), and low operation voltage less than a few volts [1-3]. In order to attain higher sensitivity to photogenerated carriers in the SOI body, further down scaling of the device is necessary. The small structure has a small capacitance, and therefore experiences a large shift of threshold voltage for a single charge. If we assume the simple expression in the linear region, the drain current is formulated as follows.

$$I_d = \frac{W}{L} \mu C_{ox} V_d (V_g - V_t) \qquad (1)$$

Since the input capacitance of the SOI MOSFET is WLC_{ox}, change in the gate voltage for a single charge is described as

$$\delta V_g = \frac{e}{LWC_{ox}} \qquad (2)$$

Note that a hole in the SOI body has the same effect as that of an electron in the gate due to the mirror image effect. As a result, the change in drain current for a single charge is expressed by

$$\delta I_d = \frac{W}{L} \mu C_{ox} V_d \delta V_g = \frac{e \mu V_d}{L^2} \quad (A/e). \qquad (3)$$

According to the Reimbold's equation [8], $1/f$ drain current noise in MOSFET is described as

$$\sqrt{S_I} = \frac{e^2 I_d}{C_{ox}} \sqrt{\frac{\lambda_{ox} N_t}{kTLWf}} = \frac{e^2 W^{1/2}}{L^{3/2}} \mu V_d (V_g - V_t) \sqrt{\frac{\lambda_{ox} N_t}{kTf}} \quad (A/\sqrt{Hz}), \qquad (4)$$

where λ_{ox} is an average tunneling length, and N_t is the concentration of slow oxide traps. By combining equations (3) and (4), we can obtain the charge sensitivity of MOSFET in the following expression.

$$\delta Q = e\sqrt{LW}(V_g - V_t) \sqrt{\frac{\lambda_{ox} N_t}{kTf}} \quad (e/\sqrt{Hz}) \qquad (5)$$

It can be conclude that we can attain smaller δQ (better charge sensitivity) by scaling down the sizes of MOSFET. In this sense, SOI fin-type field-effect transistor (FinFET) with multigate structure as an evolution of SOI MOSFET depicted in Figure 4-1 is very promising due to the superior short-channel behavior [4-5].

The purpose of this work is to study single-photon detection in SOI FinFET with single-hole sensitivity. As a result, we found that SOI FinFET could operate as single photon detector, a potential well created by $n^+p^-n^+$ junctions is used to trap photo-generated holes, which is

detected as increased electron current with a single-hole sensitivity. The evolution of the histogram toward the high-current side was clearly observed as the light intensity increases, indicating the accumulation of photogenerated holes in the body of SOI as shown in Figure 4-2. Although the peaks in the histogram of drain current are overlapped due to relatively small sensitivity to the holes, signal-to-noise ratio (SNR) is large enough to determine the position and height of each peak corresponding to the discrete number of stored holes. In addition to this single-photon detection capability, the FinFET structure could also benefit from the potentially high quantum efficiency (QE) since it includes fewer absorbing electrodes to the incident light.
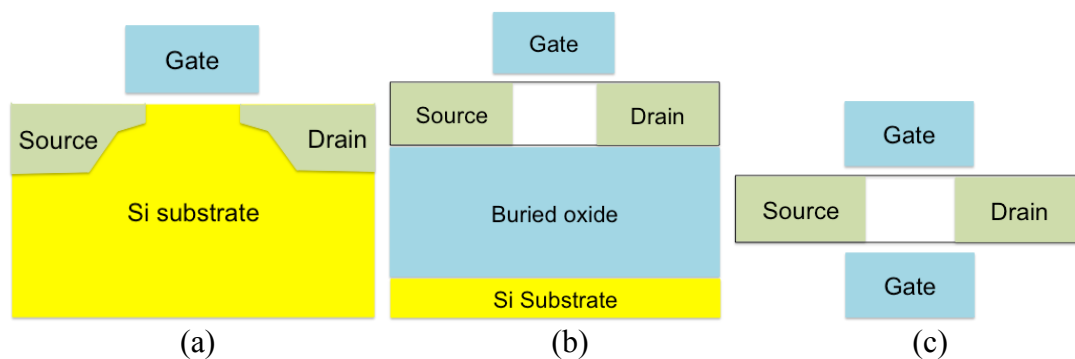
Figure 4-1 Evolution of MOSFET structures to suppress short-channel effect and enable down scaling for higher performance.
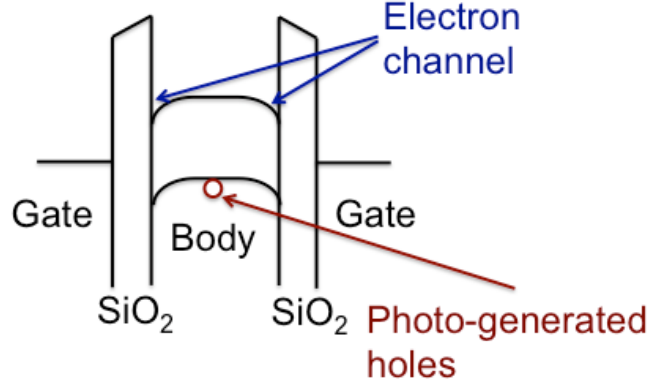
Figure 4-2 Energy band diagram in the cross-section of the SOI FinFET.

4.2 Device Structure

For this study, we fabricated and characterized SOI fin-type field-effect transistor (FinFET) with a nanometer scale. Figure 4-3 shows schematic diagram of n$^+$ poly-Si-TiN-gate n$^-$ channel SOI FinFET with intrinsic channel. Buried oxide thickness T_{BOX}, fin thickness T_{FIN}, fin height H_{FIN}, gate length L and gate oxide thickness T_{OX} are 150, 50, 40, 500 and 2.5 nm, respectively. Note that this device structure is similar to the previous device for single-photon detection with a simple structure [2], in that there is no offset region between gate and n$^+$ source/drain. In the measurement, the device is illuminated with continuous light, and the drain current waveform is analyzed. The n$^+$p$^-$n$^+$ doping structure creates the potential well to trap photo-generated holes, V_{SUB} is set to 0 V, since the bottom channel is no longer used as an electrometer to detect the

presence of the stored holes. The active region is the 40-nm-high, 50-nm-thick silicon fin with p⁻ dopant concentration less than $10^{15}\,cm^{-3}$, covered by the 500-nm-long n⁺ polycrystalline silicon (poly-Si) titanium nitride (TiN) gate.

In order to detect stored holes, $V_G > 0$ and $V_{SUB} = 0$ are selected this time for the smaller current noise, which is sensitive to the bias condition [6-15]. In this case, photogenerated holes are stored in the middle of the fin, whereas electron channel induced by the positively biased gate is used as an electrometer to detect the presence of the stored holes. Photogeneration of carriers and their recombination will modulate the electron current, and can be observed as pulses.
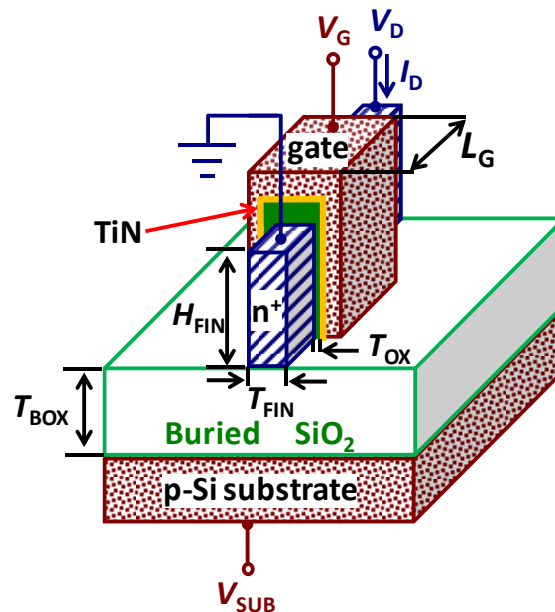
Figure 4-3 Schematic diagram of the SOI FinFET. T_{BOX}, T_{FIN}, H_{FIN}, L and T_{OX} are 150, 50, 40, 500 and 2.5 nm, respectively.

4.3 Fabrication Process

From the original wafer, devices were delineated in different sizes. After cleaning, several processes were done such as dry oxidation, resist coating, patterning, oxide etching, resist removal, top Si etching, diffusion, drive-in, and Al deposition. Such processes were repeated several times as main steps are summarized in Fig. 4-4.
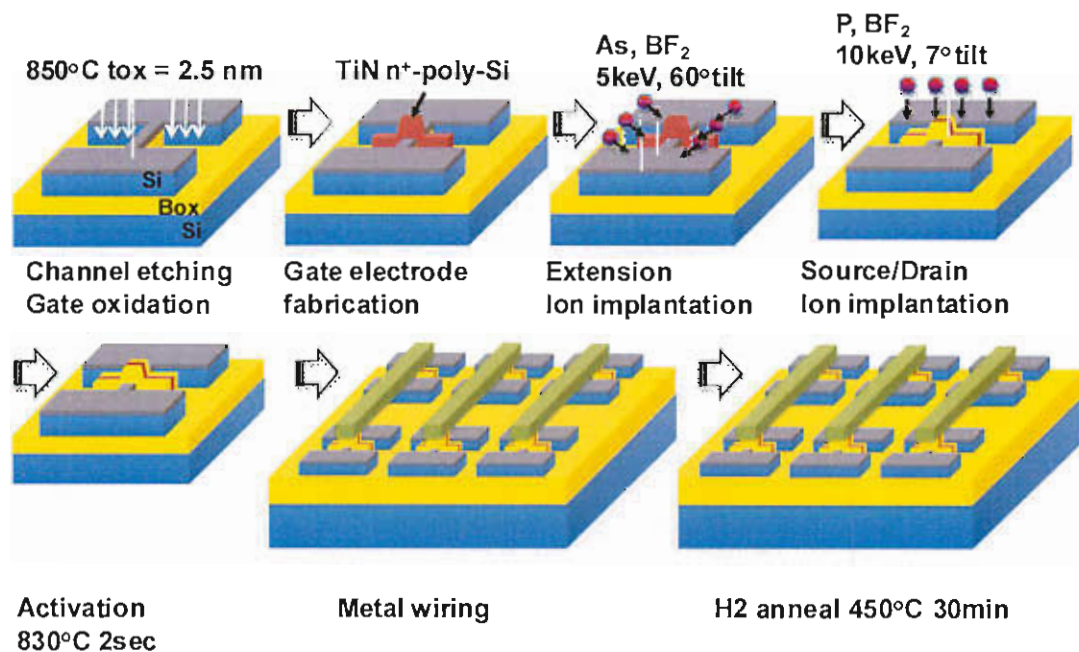
Figure 4-4 Fabrication process flow of SOI FinFET.

4.4   Measurement setup

The measurement setup for this experiment was described in Chapter 2, subchapter 2.3.2 related to the hole lifetime measurement. The measurement temperature is kept at room temperature (300K) and device is illuminated by monochromatic light with a wavelength of 550 nm.

4.5   Experimental Results and Discussion

4.5.1 Analysis of Noise Characteristics

The I_D-V_G curves with V_{SUB} as parameter from -10 to 10 V shown in Fig. 4-5. As indicated in Fig. 4-3, the characteristics are almost independent of V_{SUB} indicating that the main gate dominates the control of the channel potential. The operation point is set in the subthreshold region, where V_G= 0.218 V, V_{SUB}= 0 V and I_D ~1 nA. It was necessary to select an appropriate biasing point to reduce the drain current noise. Generally, the low-frequency noise in MOSFETs is caused by the fluctuation of the charge state of the oxide traps close to the channel [4]. This fluctuation is reflected to the drain current noise, depending on the

bias condition [5-9]. In case of SOI MOSFETs, the bias condition also affects the positions of noise-related traps, e.g. front channel, back channel, edge channel, etc. [10-12]

Since the quality of oxides is not uniform and device dependent, in SOI FinFET device, we selected V_D, V_G, and V_{SUB} of 0.05, 0.22, and 0 V, respectively, at which the noise level (i.e. the standard deviation of the drain current distribution) was minimized, and photo-generated pulse signal was clearly separated from the baseline current. We have compared drain current noise of the FinFET and planar SOI MOSFET in Fig. 4-6. It was found that the noise of the FinFET is comparable to that of planar MOSFET or rather smaller considering the general trend of

$$\sigma \propto \frac{1}{\sqrt{LW}} \text{ [13]}.$$
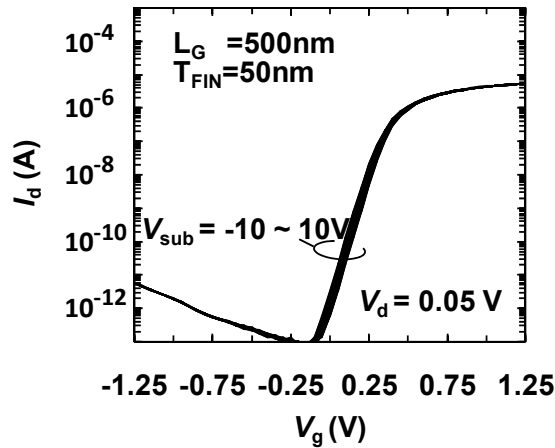
Figure 4-5 I_D-V_G characteristics with V_{SUB} as a parameter. Drain voltage V_D is kept at 50 mV. Device sizes are L = 500 nm and T_{FIN} = 50 nm.
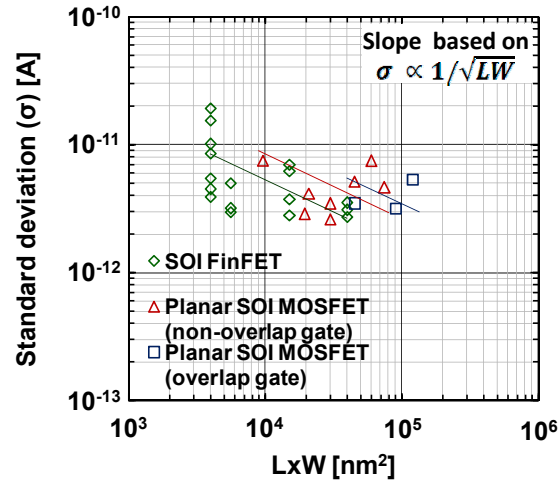
Figure 4-6 Noise characteristics of FinFET and planar SOI MOSFET. σ is the standard deviation of the drain current fluctuation for the bandwidth of 5Hz. V_D and I_D are 50mV and 1nA, respectively.

4.5.2 Analysis of Drain Current Waveform

Figure 4-7 shows typical drain current waveforms for different incident light intensities at the wavelength of 550 nm at 300 K. Baseline current is adjusted to 1 nA by V_G, and each waveform is shifted for clarity. It shows that, drain current amplitude increases as light intensity increases, though discrete current levels corresponding to the number of stored holes cannot be observed clearly. This is because the channel size of this device is larger than that of the previous one [2], resulting in lower sensitivity, i.e., smaller current change per single stored hole.
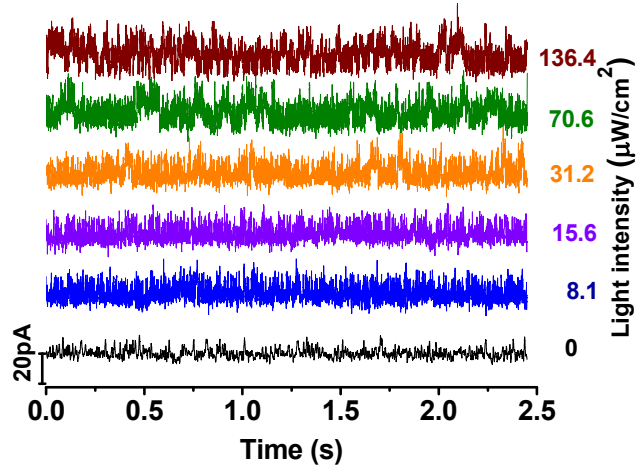
Figure 4-7 I_D waveforms at 300 K for various light intensities (λ=550 nm). Baseline current is about 1 nA, and each waveform is shifted for clarity. V_D, V_G and V_{SUB}, are 0.05, 0.218 and 0 V, respectively.

The histograms of drain currents corresponding to Figure 4-7 are shown in Figures 4-8 (a)–(f). The closed symbols are measured data and solid lines are fitting curves with Gaussian distribution. The peaks from left to right correspond to the number of stored holes of 0, 1, 2, 3 and 4. When incident light intensity increases, more and more holes are generated. Thus, the possibility of holes being stored under the gate increases, resulting in higher peaks for more stored holes.
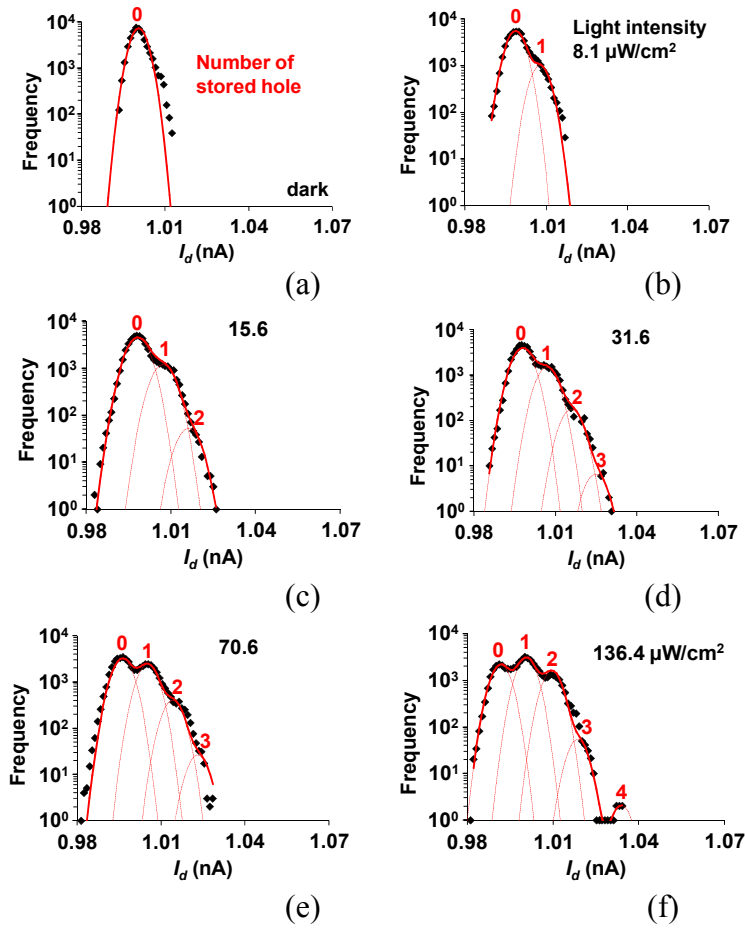
Figure 4-8 Histograms of digitized drain current corresponding to Fig. 4-7. Data acquisition time period and time step are 2.45 s and 49 μs, respectively, and 50000 2(=2.45s/49μs) data points (current values) are classified into bins with a width of 1 pA.

For the application to the single-photon detection [1], quantum efficiency (QE) of the hole generation is important, the absorption by gate TiN and polysilicon is calculated from extinction coefficient of materials. As shown in Fig. 4-9, there is proportionality between hole generation rate and incident light intensity. Here, the number of rising edges in the waveform was counted, and the nominal photon incident rate was obtained by multiplying the light intensity per area and the active area,

assuming the photosensitive area of 500×50 nm^2 ($L = 500$ nm and $T_{FIN} =$ 50 nm). The nominal quantum efficiency (QE) can be obtained from the proportionality constant, and is plotted in Figure 4-10 as a function of wavelength. Light absorption by 40-nm thick Si slab as H_{FIN} of SOI FinFET is nearly parallel to the experimental data, indicating that the spectroscopic behavior of QE is mainly governed by the Si absorption coefficient.
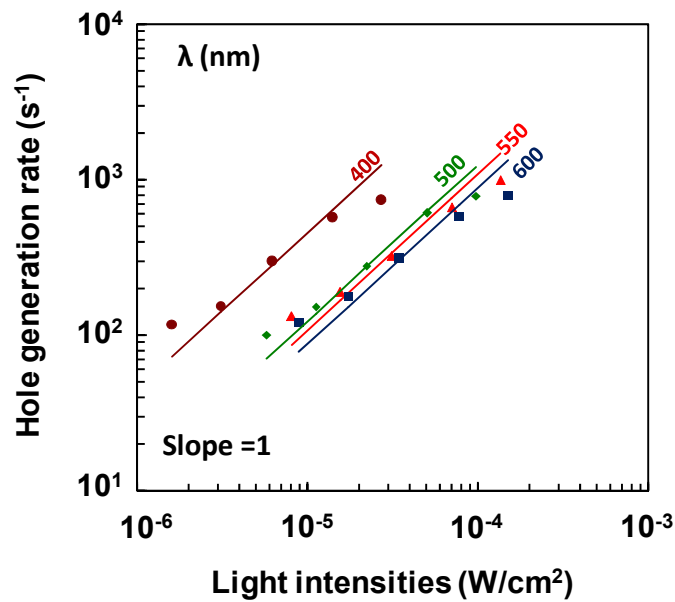
Figure 4-9 Hole generation rate as a function of incident light intensity. Symbols are measured data and solid lines are fitted ones with a slope of 1.

The highest QE is 9.0% at the shortest wavelength of 400 nm, and 1.6% at 550 nm. In our previous report of SOI MOSFET single-photon detector with offset region, the highest QE at the shortest wavelength was

1.3% [2], while, for the device without offset region, the QE is 0.11% at 550 nm [3]. We can attain significantly higher QE in SOI FinFET due to the SOI FinFET structure that is not covered by upper gate and allow light illumination to be more directly absorbed in active area than the case in the previous devices.

Although the QE was improved, we could not attain better charge sensitivity or dynamic range as a photon detector. Further investigation on the effects of device structure and dimensions for higher charge sensitivity is anticipated, and a novel technology such as surface plasmon antenna needs to be introduced for higher QE.
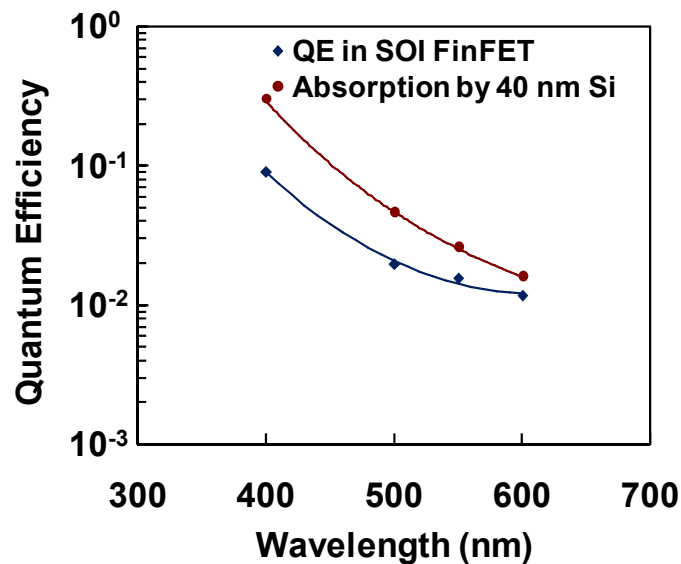
Figure 4-10 Nominal quantum efficiency with respect to the wavelength. Light absorption of 40 nm Si slab calculated from absorption coefficient is also shown.

4.5.3 Analysis Hole Lifetime

Figure 4-11 (a) shows probabilities of states f_i corresponding to the number of stored holes i as a function of count rate, namely, hole generation rate R. The behavior can be explained by the state transition diagram in Fig. 5-12 (b).
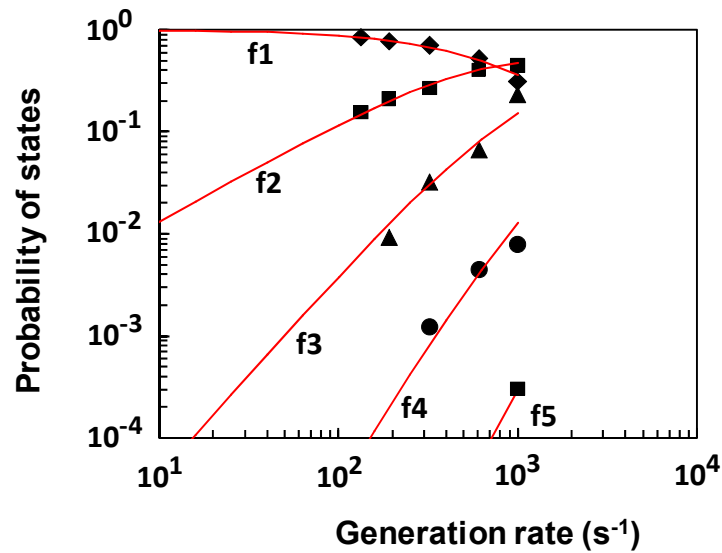
(a)
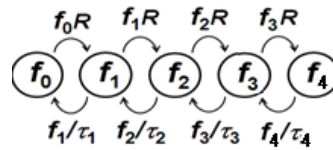
(b)

Figure 4-11 Probability of states obtained from Fig. 4-6 as a function of count rate, namely, hole generation rate R. State f_0, f_1, f_2, and f_3 correspond to zero, one, two and three stored holes, respectively. Fitting to the theoretical curve (solid lines) is made based on the filled data points. (b) State transition diagram to explain (a).
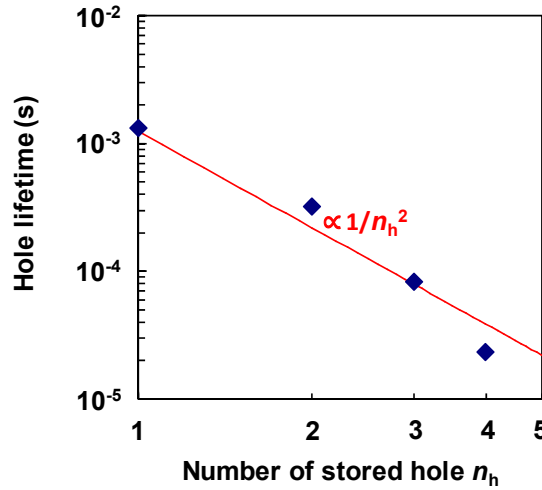
Figure 4-12 Hole lifetime in SOI FinFET as a function of number of stored holes n_h.

The theoretical curves (solid lines) are derived from the rate equations under steady-state condition, $f_i/\tau_1 = f_{i-1}R$ and $\sum f_i = 1$, where τ_i is the hole lifetime for the number of stored holes of i (=0, 1, 2, 3 and 4) [2]. Figure 4-12 shows the hole lifetime of SOI FinFET as a function of number of stored holes n_h. We can see hole lifetime in SOI FinFET has stronger n_h dependence than the case with planar SOI MOSFET, and seems to be inversely proportional to the square of the number of stored hole n_h. This may be caused by the shallow potential well for the hole storage, leading to the early saturation of the hole number.

Conclusion

In conclusion, a SOI fin-type field effect transistor (FinFET) with multigate structure was investigated as a photon detector *for the first time*, expecting the improved performance of the MOSFET-based single-photon detector. We could successfully confirm the photodetection capability, in that the drain current histogram evolved toward the high-current side as the light intensity increased, reflecting the accumulation of photogenerated holes. Although the QE is improved to 9.0% at $\lambda = 400$ nm, we could not attain better charge sensitivity or dynamic range as a photon detector. Further investigation on the effects of device structure and dimensions is anticipated for higher charge sensitivity.

References

[1]   H. Inokawa, W. Du, M. Kawai, H. Satoh, A. Ono, and V. Singh, "Single-Photon Detector Based on MOSFET Electrometer with Single-Electron Sensitivity," *Adv. Mater. Res.*, 222, pp. 3-7, 2011.

[2]   W. Du, H. Inokawa, H. Satoh, and A. Ono, "SOI metal-oxide-semiconductor field-effect transistor photon detector based on single-hole counting,"*Opt. Lett* 36(15), pp. 2800-2802, 2011.

[3]   W. Du, H. Inokawa, H. Satoh, and A. Ono, "Single-Photon Detection by a Simple Silicon-on-Insulator Metal-Oxide-Semiconductor Field-Effect Transistor," *Jpn. J. Appl. Phys.*, 51(6), pp. 06FE01-1-06FE01-4, 2012.

[4]   T. Irisawa , K. Okano , T. Horiuchi , H. Itokawa , I. Mizushima , K. Usuda , T. Tezuka , N. Sugiyama and S. Takagi "Electron mobility and short-channel device characteristics of SOI FinFETs with uniaxially strained (110) channels," *IEEE Trans. Electron Devices*, 56, 8, pp. 1651 -1658, 2009.

[5]   T. Hayashida, K. Endo, Liu Yongxun, S. O'uchi, T. Matsukawa, W. Mizubayashi, S. Migita, Y Morita, H. Ota, H. Hashiguchi, D. Kosemura, T. Kamei, J. Tsukada, Y. Ishikawa, H. Yamauchi, A. Ogura, M. Masahara, "Fin-Height Effect on Poly-Si/PVD-TiN

Stacked-Gate FinFET Performance," *IEEE Trans. Elec. Dev.* 59, pp. 647 – 653, 2012.

[6]   Sh. Kogan, "Electronic Noise and Fluctuations in Solids," (Cambridge University Press, Cambridge, U.K., 1996) p. 234.

[7]   G. Ghibaudo, "A simple derivation of Reimbold's drain current spectrum formula for flicker noise in MOSFETs," *Solid-State Electron*, 30, p. 1037, 1987.

[8]   G. Reimbold, "Modified 1/f trapping noise theory and experiments in MOS transistors biased from weak to strong inversion-influence of interface states," *IEEE Trans. Electron Devices*, 31, pp. 1190-1198, 1984.

[9]   C. Jakobson, I. Bloom, and Y. Nemirovsky, "1/f Noise in CMOS Transistors for Analog Applications from Subthreshold to Saturation," *Solid-State Electron*, 42, pp. 1807-1817, 1998.

[10]   E. Simoen and C. Claeys, "On the flicker noise in submicron silicon MOSFETs," *Solid-State Electron*, 43, pp. 865–882, 1999.

[11]   Y. Nemirovsky, I. Brouk, and C. G. Jakobson, "1/f noise in CMOS transistors for analog applications," *IEEE Trans. Electron Devices,* 48, pp. 921–927, 2001.

[12]   S. Cristoloveanu and Sheng S. Li, "Electrical Characterization of Silicon-on-Insulator Materials and Devices," (Kluwer, Boston, MA, 1995) p. 297.

[13] T. Elewa, B. Boukriss, H.S. Haddara, A. Chovet, and S. Cristoloveanu, "Low-frequency noise in depletion-mode SIMOX MOS transistors," *IEEE Trans. Electron Devices*, 38, p. 323, 1991.

[14] T. Elewa, B. Kleveland, S. Cristoloveanu, B. Boukriss, and A. Chovet, "Detailed analysis of edge effects in SIMOX-MOS transistors," *IEEE Trans. Electron Devices*, 39, pp. 874-882, 1992.

[15] S. Christensson, I. Lundstrom, C. Svensson, "Low frequency noise in MOS transistors-I Theory," *Solid State Electron*, 11, pp. 797-812, 1968.

Chapter 5

SUMMARY AND FINAL CONCLUSION

5.1   Summary

The main goal of this work is to realize the SOI MOSFET photon detector based on single-hole counting, which has clear advantages over and can outperform the conventional single-photon detectors. First in this thesis, we investigated the effect of substrate bias on noise and hole lifetime in the body SOI MOSFET photon detector to optimize the operation condition to attain high-speed operation. After investigating the required charge sensitivity for single-charge counting, we researched the possibility of SOI fin-type field-effect transistor as a photon detector.

Chapter 1 of this thesis presented the background of the research related to single-photon detector, describing the key advances that set the grounds for photon detection by SOI MOSFET. Some reports on conventional single-photon detectors including ones based on single-charge counting are summarized. The motivation of the present research is outlined, and synopsis of each chapter is described. This chapter

provided the basic knowledge required to understand the mechanism responsible for our experimental observations.

Chapter 2, effect of substrate bias on the low-frequency noise and hole lifetime in SOI MOSFET single-photon detector was investigated to optimize the operation condition in terms of high-speed operation. The noise becomes minimum at around the transition point between front- and back-channel operations when the substrate voltage is varied, and increases largely on both negative and positive sides of the substrate voltage showing peculiar Lorentzian (generation-recombination) noise spectra. Hole lifetime is evaluated by the analysis of drain current histogram at different substrate voltages. It is found that the peaks in the histogram corresponding to the larger number of stored holes become higher as the substrate bias becomes larger. This can be attributed to the prolonged lifetime caused by the higher electric field inside the body of SOI MOSFET. It can be concluded that, once the inversion channel is induced for detection of the photogenerated holes, the small absolute substrate bias is favorable for short lifetime and low noise, leading to high-speed operation.

Chapter 3, the attainable performance by the SOI MOSFET photon detector is investigated, based on the newly developed model of the output waveforms and the signal-processing algorithm. The photogeneration and recombination are simulated as independent Poisson

processes, whose timings are set by random numbers. In order to detect the events of hole generation by photon incidence and recombination, the output signal is differentiated, and positive and negative peaks are associated with the respective events.

Based on the linearity between detected and generated rates of holes, and detected rate under null generation for different noise levels and sampling frequencies, correlation between maximum and dark count rates is established for a given charge sensitivity. For example, a record-high dynamic range of 178 dB (maximum and dark count rates of 7.6 Ms^{-1} and 0.01 s^{-1}, respectively) can be attained by the use of a state-of-the-art charge sensor with sensitivity of 1×10^{-5} e/$\sqrt{\text{Hz}}$ [3] at the sampling frequency of 150 MHz.

Chapter 4, we successfully confirm the photon detection by SOI fin-type field-effect transistor (FinFET). A potential well created by $n^+p^-n^+$ junctions is used to store photogenerated holes, which are detected as increased electron current with a single-hole sensitivity. As oppose to the expectation of higher charge sensitivity, peaks in histograms of drain current are overlapped, but the signal-to-noise ratio (SNR) is large enough to determine the position and height of each peak corresponding to the discrete number of stored holes. In addition to this single-photon detection capability, the FinFET structure could also benefit from the

potentially high quantum efficiency (QE) since it includes fewer absorbing electrodes to the incident light.

5.2 Unresolved Issues

I have successfully demonstrated the effect substrate bias on noise and minority carrier lifetime on SOI MOSFET single-photon detector, and the single-hole detection by the SOI fin-type field-effect transistor (FinFET). A number of issues, however, remain unresolved. Below is a list of such issues that require further studies before clarification.

1. *Low sensitivity to a hole*. Peaks in histograms of drain current are overlapped due to relatively small sensitivity to the holes.

2. *Small signal to noise ratio (SNR)*. As oppose to the expectation, SNR of SOI FinFET is much smaller. Structural and dimensional optimization of the device remains to be done.

3. *Small quantum efficiency (QE) and area of detection*. This is a general requirement on photodetectors, but is not fully addressed in this thesis. Since the volume and area for light absorption is inevitably small for detectors with high charge sensitivity, a novel technology such as surface plasmon antenna needs to be introduced.

5.3 Final Conclusion and Future Prospects

The research goal presented in the thesis was utilization of single hole sensitivity in the body of SOI to detect single photons. This goal has been successfully achieved. Effect of substrate bias on noise and minority carrier lifetime SOI MOSFET photon detector was analyzed to optimize the operation condition, and photon detection by SOI fin-type field-effect transistor has been proved at room temperature. This result may give insights for future photon detector based single-charge counting at room temperature.

The next goal is to realize performance higher than the conventional ones in overall aspects covering dark and maximum count rates, quantum efficiency, operation voltage, photon number resolution, etc.

Appendix

Source code program of performance estimation

```matlab
% Script File: Photon5e.m

% Error in Waveform Generation is corrected

% Simple thresholding (md=0) for data processing (counting events)

% Digital filter to reflect the freq. response of pre-amplifier

% E3_Rec, E3_Gen (sum of rec and gen events) New para

% Adapted from randapal29.m by Nakagami-kun

clear all

close all

%

y1=4240;  % Hole generation rate [frequency] [1/s]******************

y2=4240;  % Recombination rate when the number of stored hole is one
[1/s]*************

s=1.5E5;  % Total number of generation / recombination events ex. 25000, 1.5E5

E=zeros(s,1);   % Declaration of matrix size (necessary for speeding up the
calculation)

H=zeros(s,1);

T=zeros(s,1);

h=0;      % Initial value of the number of stored hole

n=1;      % Counter of the events

% ****************

% Step1: Generation of the event series

% ****************

for k1=1:s

  r2=rand(1);

  t2=(-1/y1)*log(r2); % Hole generation

  if(h==0)

      t3=2*t2;

  end

  if(h>0)

  r3=rand(1);

  t3=(-1/(y2*h))*log(r3); % Recombination

%  t3=(-1/(y2))*log(r3); % Recombination (constant lifetime)

  end

  if(t3>t2)  % In case of hole generation

   T(n,1)=t2;

   E(n,1)=1;
```

```
      end
    if(t2>=t3)  % In case of recombination
      T(n,1)=t3;
      E(n,1)=-1;
    end
    H(n,1)=h;  % Number of stored hole just before the event
      h=H(n,1)+E(n,1);
      n=n+1;
end
% Statistics
nh_max=max(H);
% nGen, nRec
bins=-1:2:1;
[nRecGen,xRecGen]=hist(E,bins);
% nHole
bins=0:1:nh_max;
[nHole,xHole]=hist(H,bins);
% File output of Step1
fid1=fopen('C:\MATLABR11\MFILES\single-photon\step1.txt','w');
fprintf(fid1,'Step1 output of Photon5e.m\n');
fprintf(fid1,'y1 %13.5e y2 %13.5e s %d\n',y1,y2,s);
fprintf(fid1,'n E(n) T(n) H(n)\n');
for n=1:s
    fprintf(fid1,'%d %d %13.5e %d\n',n,E(n,1),T(n,1),H(n,1));
end
fprintf(fid1,'*****Statistics*****\n');
fprintf(fid1,'nh_max %d\n',nh_max);
fprintf(fid1,'xRecGen %d %d\n',xRecGen);
fprintf(fid1,'nRecGen %d %d\n',nRecGen);
fprintf(fid1,'xHole\n');
fprintf(fid1,'%d\n',xHole);
fprintf(fid1,'nHole\n');
fprintf(fid1,'%d\n',nHole);
status=fclose(fid1);
%pause
% ****************
% Step2: Waveform generation with noise
% ****************
```

Page | 92

```matlab
step=1.0E-6;           % Time step (sampling period) [s]
***************************************

time=10.0;             % End time [s] ************************

x=round(time/step);    % Number of time steps (rounded to the nearest integer)

xx=step:step:time;

wave=zeros(x,1);    % Declaration of matrix size (necessary for speeding up the
calculation)

dwave=zeros(x,1);

I=1.0;          % Base line of the output waveform

dI=1.0;       % Step height of the output waveform (corresponding to a single hole)

noise=4.964;    % Noise stnadard deviation *************************

wave_out=0;    % File output of the waveform data [Yes (1), No (0)]
***************************

n1=1;                  % Initialization of the event (change in the number of stored
hole) counter

t0=T(n1,1);            % Initialization of time (time for the 1st event is entered)

% Waveform Generation

for k=1:x

    while xx(1,k)>t0

        n1=n1+1;

        t0=t0+T(n1,1);

    end

    wave(k,1)=I+dI*H(n1,1)+noise*randn(1);

end

% ***************

% Digital filer

% ***************

f_cutoff=800;   % Cutoff freq. ******************************

if f_cutoff>0

  tau=1/(2*pi*f_cutoff*step);

  wa=1/(1+tau);

  wb=tau/(1+tau);

  wave0=0.0;

  for k=1:x

    wave0=wb*wave0+wa*wave(k,1);

    wave(k,1)=wave0;

  end

end

% ***************

% Statistics

n_event=n1;
```

```matlab
E2=E(1:n_event,1);

H2=H(1:n_event,1);

nh2_max=max(H2);

% nGen2, nRec2

bins=-1:2:1;

[nRecGen2,xRecGen2]=hist(E2,bins)

% nHole2

bins=0:1:nh2_max;

[nHole2,xHole2]=hist(H2,bins);

% Waveform

wave_max=(round(max(wave)*20)+1)/20;

wave_min=(round(min(wave)*20)-1)/20;

xxx=wave_min:0.05:wave_max;

[nWave,xWave]=hist(wave,xxx);

% Generation of graphs

figure          % Plot of the waveform

plot(xx,wave);

figure          % Plot of the histogram

bar(xWave,nWave)

%hist(wave,xxx)

% File output of Step2

fid2=fopen('C:\MATLABR11\MFILES\single-photon\step2.txt','w');

fprintf(fid2,'Step2 output of Photon5e.m\n');

fprintf(fid2,'y1 %13.5e y2 %13.5e s %d f_cutoff %13.5e\n',y1,y2,s,f_cutoff);

fprintf(fid2,'step %13.5e time %13.5e I %13.5e dI %13.5e
noise %13.5e\n',step,time,I,dI,noise);

if wave_out==1

    fprintf(fid2,'xx wave\n');

    for k=1:x

        fprintf(fid2,'%13.5e %13.5e\n',xx(1,k),wave(k,1));

    end

end

fprintf(fid2,'*****Statistics*****\n');

fprintf(fid2,'n_event %d nh2_max %d\n',n_event,nh2_max);

fprintf(fid2,'xRecGen2 %d %d\n',xRecGen2);

fprintf(fid2,'nRecGen2 %d %d\n',nRecGen2);

fprintf(fid2,'xHole2\n');

fprintf(fid2,'%d\n',xHole2);

fprintf(fid2,'nHole2\n');
```

Page | 94

```matlab
        fprintf(fid2,'%d\n',nHole2);

        fprintf(fid2,'xWave\n');

        fprintf(fid2,'%d\n',xWave);

        fprintf(fid2,'nWave\n');

        fprintf(fid2,'%d\n',nWave);

        status=fclose(fid2);

        % ****************

        % Step3: Data processing of the generated waveform

        % ****************

        % k: Counter of the time step (1~x)

        % xx(1,k),wave(k,1) Waveform data (time, amplitude)

        % Step height in the waveform should be normalized to 1.0

        % E3(nE,1) Generated holes in an event (>0), Recombined holes (<0)

        % time3(nE,1) Time of event (hole generation / recombination)

        % dwave(nE,1) differentiated waveforem

        % Smoothed differentiation
        md=0;      % degree of smoothing (md>=1, integer) k=1+md ~ x-md  **************
        if md==0
            % Simple thresholding w/o relying on differentiation
            nE=0;     % Event counter
            for k=1:x-1
                d_wave=wave(k+1,1)-wave(k,1);
                d_rwave=round(wave(k+1,1))-round(wave(k,1));
                nGR_base=round(abs(d_wave)-0.5); % Base number of GR in a time step (0>=0)
                ad_r=abs(d_rwave)-nGR_base;
                d0_r=round(wave(k,1))-wave(k,1);
                d1_r=round(wave(k+1,1))-wave(k+1,1);
        %     if ((d0_r*d1_r>0)&(ad_r==1))|((d0_r*d1_r<0)&(ad_r==0))
                if ad_r==1
                    nGR=nGR_base+1;
                else
                    nGR=nGR_base;
                end
                if nGR>=1
                    nE=nE+1;
                    E3(nE,1)=sign(d_wave)*nGR;
                    time3(nE,1)=(xx(1,k)+xx(1,k+1))/2;
                end
```

```
        end

else

NORM=md*(md+1)*(2*md+1)/3;       % Normalization constant

for k=1:x

    if (k<md+1)|(k>x-md)

        dwave(k,1)=0;

    else

        dw=0;

        for L=-md:md

            dw=L*wave(k+L,1)+dw;

        end

        dwave(k,1)=dw/NORM;

    end

end

% Detection of events

dw_th=3/4/(2*md+1);      % Threshold of detection

nE=0;      % Event counter

dw_integ=0;    % Intergation of peak values

for k=1:x

    if dw_integ==0

        if (dwave(k,1)>dw_th)|(dwave(k,1)<-dw_th)

            dw_integ=dwave(k,1);    % Start of integration

        end

    else

        if dw_integ>0

            if dwave(k,1)>dw_th

                dw_integ=dw_integ+dwave(k,1);    % Continue to integrate

            else

                if round(dw_integ)>=1

                    nE=nE+1;

                    E3(nE,1)=round(dw_integ);

                    time3(nE,1)=xx(1,k);

                end

                dw_integ=0;

                if dwave(k,1)<-dw_th

                    dw_integ=dwave(k,1);

                end

            end

        else
```

```matlab
            if dwave(k,1)<-dw_th
                dw_integ=dw_integ+dwave(k,1);    % Continue to integrate
            else
                if round(dw_integ)<=-1
                    nE=nE+1;
                    E3(nE,1)=round(dw_integ);
                    time3(nE,1)=xx(1,k);
                end
                dw_integ=0;
                if dwave(k,1)>dw_th
                    dw_integ=dwave(k,1);
                end
            end
        end
    end
end
end
% Statistics
nE_max=nE;    % Number of events
E3_min=min(E3);
E3_max=max(E3);
% Hole recombination/generation
bins=E3_min:1:E3_max;
[nE3,xE3]=hist(E3,bins)
E3_RecGen=nE3.*xE3;
E3_Rec=-sum(E3_RecGen(1,1:-E3_min))
E3_Gen=sum(E3_RecGen(1,-E3_min+2:-E3_min+E3_max+1))
% File output of Step3
fid3=fopen('C:\MATLABR11\MFILES\single-photon\step3.txt','w');
fprintf(fid3,'Step3 output of Photon5e.m\n');
fprintf(fid3,'md %d nE_max %d E3_min %d E3_mx %d\n',md,nE_max,E3_min,E3_max);
fprintf(fid3,'xE3\n');
fprintf(fid3,'%d\n',xE3);
fprintf(fid3,'nE3\n');
fprintf(fid3,'%d\n',nE3);
fprintf(fid3,'E3_Rec %d E3_Gen %d\n',E3_Rec,E3_Gen);
fprintf(fid3,'*** List of all events ***\n');
fprintf(fid3,'nE time3(nE) E3(nE)\n');
```

```
for nE=1:nE_max

    fprintf(fid3,'%d %13.5e %d\n',nE,time3(nE,1),E3(nE,1));

end

if md>=1

    fprintf(fid3,'*** Differentiated waveform ***\n');

    fprintf(fid3,'xx dwave\n');

    for k=1:x

        fprintf(fid3,'%13.5e %13.5e\n',xx(1,k),dwave(k,1));

    end

end

status=fclose(fid3);

%pause
```

List of Publications

1.1 Journal Papers and Proceedings

1) D.S.C. Putranto, W. Du, H. Satoh, A. Ono, P.S. Priambodo, D. Hartanto, and H. Inokawa, "Analysis of Hole Lifetime in SOI MOSFET Single-Photon Detector". Makara Journal of Technology Series, Vol 17, No 1, pp.7-10 (2013).

2) D.S.C. Putranto, P.S. Priambodo, D. Hartanto, W. Du, H. Satoh, A. Ono, and H. Inokawa, "Effects of substrate voltage on noise characteristics and hole lifetime in SOI metal-oxide-semiconductor field-effect transistor photon detector," Optics express, Vol. 22, No. 18, pp. 22072-22079 (2014).

3) D.S.C. Putranto, K. Endo, M. Masahara, H. Satoh, A. Ono, P.S. Priambodo, D. Hartanto, and H. Inokawa, "Single-Photon Detection by a Silicon-on-Insulator Fin-Type Field-Effect Transistor". Applied Physic Express, to be submitted.

4) D.S.C. Putranto, W. Du, H. Satoh, A. Ono, P.S. Priambodo, D. Hartanto, and H. Inokawa, "Substrate Bias Effects on Noise and Minority Carrier Lifetime in SOI MOSFET Single Photon

Detector", Proceeding of the 13th International Conference on QIR, pp. 908-911, Yogyakarta, Indonesia (2013).

5) (Invited) H. Inokawa, H. Satoh, A. Ono, <u>D.S.C. Putranto</u>, and T. Ajay, "Recent Advances in Photodetectors Based on Silicon-On-Insulator", Proceeding of The 2013 Korean-Japanese Students Workshop, pp. 5-9 (2013).

6) H. Inokawa, <u>D.S.C. Putranto,</u> W. Du, H. Satoh, A. Ono, P.S. Priambodo, and D. Hartanto, "Evolution of Photodetectors by Silicon-On-Insulator Material", Proceeding of the 13th International Conference on QIR, pp. 890-894, Yogyakarta, Indonesia (2013).

7) W. Du, <u>D.S.C. Putranto</u>, H. Satoh, A. Ono, P.S. Priambodo, D. Hartanto, and H. Inokawa, "Optoelectrical Lifetime Evaluation of Single Holes in SOI MOSFET", IEEE Silicon Nanoelectronics Workshop (SNW), pp. 149-150, Honolulu, Hawaii (2012).

8) H. Inokawa, H. Satoh, A. Ono and <u>D.S.C. Putranto</u>, "Recent Progress in photodetector based on Silicon on Insulator", Proceeding of International Conference on Optoelectronis and Microelectronics Technology and Application, Invited talks, pp. 6-7 Tianjin, China. (Nov. 12-14, 2014).

1.2 List of Conferences and Symposiums

1.2.1 International Conferences and Symposiums

1) <u>D.S.C. Putranto,</u> W. Du, H. Satoh, A. Ono, P.S. Priambodo, D. Hartanto, and H. Inokawa, "Substrate Bias Effects on Noise and Minority Carrier Lifetime in SOI MOSFET Single-Photon Detector", 13th International Conference on Quality in Research (QiR) 2013, pp. 908-911, Yogyakarta, Indonesia (Jun. 25-28, 2013).

2) <u>D.S.C. Putranto,</u> W. Du, H. Satoh, A. Ono, P.S. Priambodo, D. Hartanto, and H. Inokawa, "Analysis of Hole Lifetime in SOI MOSFET Single-Photon Detector SOI MOSFET", International Conference on Nano Electronics Research and Education 2012, paper # A2.05 p.19, Bali, Indonesia (Jul. 8-10, 2012).

3) <u>D.S.C. Putranto,</u> W. Du, H. Satoh, A. Ono, P.S. Priambodo, D. Hartanto, and H. Inokawa, "Analysis of Noise in SOI MOSFET for Single-Photon Detector", 14th Takanayagi Symposium, pp. s4-10-1~4, Hamamatsu, Japan (Nov. 27-28, 2012).

4) <u>D.S.C. Putranto,</u> K. Endo, M. Masahara, H. Satoh, A. Ono, P.S. Priambodo, D. Hartanto and H. Inokawa, "Photodetection Characteristics of Fin-Type Field-Effect Transistors", 15th

Takanayagi Symposium, pp. s4-10-1~4, Hamamatsu, Japan (Nov. 12-13, 2013).

5) W. Du, D.S.C. Putranto, H. Satoh, A. Ono, P.S. Priambodo, D. Hartanto, and H. Inokawa, "Optoelectrical Lifetime Evaluation of Single Holes in SOI MOSFET", IEEE Silicon Nanoelectronics Workshop (SNW) , pp. 149-150, Honolulu, Hawai (Jun. 10-11, 2012).

6) H. Inokawa, Y. Nakagami, D.S.C. Putranto, H. Satoh, A. Ono, P.S. Priambodo, and D. Hartanto, "Performance Estimation of SOI MOSFET Single-Photon Detector", 12th International Conference on Global Research and Education, p. 24, Sofia, Bulgaria (Sep. 23-27, 2013).

7) (Invited) H. Inokawa, H. Satoh, A. Ono, D.S.C. Putranto, and T. Ajay, "Recent Advances in Photodetectors Based on Silicon-On-Insulator", The 2013 Korean-Japanese Students Workshop, Hamamatsu, Japan (Oct. 31- Nov. 1, 2013).

8) (Invited) H. Inokawa, H. Satoh, A. Ono and D.S.C. Putranto, "Recent Progress in photodetector based on Silicon on Insulator", Proceeding of International Conference on Optoelectronis and Microelectronics Technology and Application, pp. 6-7 Tianjin, China. (Nov. 12-14, 2014).

1.2.2 *National Conferences and Symposiums*

1) D.S.C. Putranto, W. Du, H. Satoh, A. Ono, P.S. Priambodo, D. Hartanto, and H. Inokawa, "Noise Characteristics of SOI MOSFET for Single-Photon Detection", JSAP 2013, Spring Meeting, 29a-G9-11, Atsugi, Japan (Mar. 27-30, 2013).

2) D.S.C. Putranto, K. Endo, M. Masahara, H. Satoh, A. Ono, P.S. Priambodo, D. Hartanto and H. Inokawa, "Analysis of Photoresponse in SOI FinFET", JSAP 2013, Fall Meeting, 20a-C8-9, Kyoto, Japan (Sep. 16-20, 2013).

3) Y. Nakagami, D.S.C. Putranto, H. Satoh, A. Ono, P.S. Priambodo, D. Hartanto and H. Inokawa, " Potential Performance of SOI MOSFET Single-Photon Detector", JSAP 2014, Spring Meeting, 19p-F12-3, Sagamihara, Japan (Mar. 17-20, 2014).